The Secondary Permeability of "Impervious" Cover in Austin, Texas

by

Thomas Jefferson Wiles, B.A.

Thesis

Presented to the Faculty of the Graduate School of

The University of Texas at Austin

in Partial Fulfillment

of the Requirements

for the Degree of

Master of Science in Geological Sciences

The University of Texas at Austin

December, 2007

The Secondary Permeability of “Impervious” Cover in Austin, Texas

Approved by
Supervising Committee:

_____

_____

_____

Dedication

To my sweet and understanding wife Melissa for her support during my time of change.

Acknowledgements

I would like to express my gratitude to my friend and advisor Jack Sharp for his keen insights and gentle persuasion. Thanks for having the patience to let me find my own way. I would also like to thank my committee members Mark Helper, who walked by my side as I was being escorted from my seat at the Sam Houston State game, and Randy Marrett (Business hours are over baby!). I am grateful for the support and advice of my friends and classmates, Al, Brad, Trevor, Bea, Don, Marcus, Megan, and Audrey. I have been inspired to be a better geologist by my professors Earle McBride, Kitty Milliken, Bob Folk, Mark Cloos, Phil Bennett, and the late Bob Goldhammer. Finally, I would like to thank my family: Melissa, you have been my partner and an inspiration; Mom, thank you for the countless hours of editing and worrying; Pop, you're the best man I know thank you for all those Saturday afternoons at Antoine's; My brothers and sisters Julie, Philip, Jocelyn, Matthew, Martha, and Elizabeth, what a wonderful life we've had together.

December 7, 2007

Abstract

The Secondary Permeability of “Impervious” Cover in Austin, Texas

Thomas Jefferson Wiles, M.S. Geo. Sci.

The University of Texas at Austin, 2007

Supervisor: John M. Sharp Jr.

The term "impervious" is commonly used in urban settings to describe the permeability of buildings, roads, and parking lots. When estimating recharge to an aquifer underlying an urbanized area, impervious cover becomes a prime consideration. It is commonly assumed that an increase in impervious cover leads to a decrease in precipitation recharge. However, even a cursory glance at most roads, sidewalks, or parking lots reveals that, far from being impervious, there are abundant fractures that may provide avenues of infiltration. For this study, method was developed to determine the secondary permeability of pavements using a double ring infiltrometer to measure the infiltration rate of water into fractured pavements. Linear extrapolation is employed to determine the infiltration rate as the water depth approaches zero, which is used as a proxy for hydraulic conductivity by assuming that the gradient is unity.

Data were collected on concrete and asphalt pavements located in Austin, Texas, at each point a fracture or expansion joint intersected along 30-meter scanlines. By dividing the sum of the discharges for each fracture by the area represented by the scanline we are able to determine the equivalent-porous-media hydraulic conductivity. The equivalent hydraulic conductivities for discrete fractures were found to range at least three orders of magnitude, from $>10^{-2}$ to 10^{-5} cm/sec; scanline hydraulic conductivities range two orders of magnitude from $>10^{-4}$ to 10^{-6} cm/sec; permeability along the scanlines tends to be dominated by one or two highly conductive fractures; and the hydraulic conductivity of the entire paved surface is $5.9 \cdot 10^{-5}$ cm/s. Both apertures and point hydraulic conductivities were found to have logarithmic distributions but cross plots demonstrated no correlation, which indicated that a combination of the fill material and sub grade, not the fractures and expansion joints themselves, limit infiltration. By multiplying the paved surface hydraulic conductivity by the time the surface can be expected to be saturated, we find that 170 mm or 21 percent of mean annual rainfall is available as potential recharge. When coupled with an enhanced subsurface permeability structure resulting from the installation of utilities and the reduction of evapotranspiration from the reduction of vegetation, the net effect of roads and parking lots could be an increase in precipitation recharge.

Table of Contents

List of Tables xii

List of Figures xiii

CHAPTER 1: INTRODUCTION 1

Effects of Urbanization 2

Urban Recharge 2

Recharge Misconceptions 3

Rising Water Tables 4

Urban infiltration 4

Rainfall-Runoff Relationships 5

Preferential Flow Paths 7

Fracture Flow 7

Purpose and Scope of Work 8

CHAPTER 2: METHODS 14

Location and Hydrogeologic Setting 14

Geology 14

Land Use 15

Individual Site Selection 15

Simplifying Assumption 16

Phase I – Proof of Concept and Methods Development 16

Initial Experiment Location 16

Initial Experiment Design 17

Initial Experiment Apparatus 17

Initial Experiment Data Collection 18

Initial Method Problems and Refinement 18

Phase II – Bench Testing 19

Bench-Testing Apparatus 19

Bench Test Results and Method Refinement 20

Phase III – 4/8 Method....20
4/8 Method Data Collection....20
4/8 Method Data Analysis....21
4/8 Method Problems and Refinement....22
Phase IV – The Wiles Rational Method....22
Method Rationale....23
Rational Method Data Collection....23
Rational Method Data Analysis....23
CHAPTER 3: RESULTS....30
Hydrogeologic Summary of Scanlines....30
Hydogeologic Summary of Point Data....30
Asphalt Pavements....31
Concrete Pavements....31
Combination Pavements....32
Hydrogeologic Summary of Cumulative Scanline Data....32
Point Hydraulic Conductivity Distribution....33
Attributes of Fracture and Joint Population....33
Histograms....33
Frequency Distributions....34
Fracture and Joint Trends....34
Effect of Aperture on Equivalent Hydraulic Conductivity....34
Time Discharge Relation....35
CHAPTER 4: INTERPRETATION AND DISCUSSION....51
Direct Recharge Transitions to Localized Recharge....51
Calculation of Potential Recharge....51
Precipitation Data....52
Potential Recharge....53
Evapotranspiration....53
Urban Karst....54
Utility Trench Permeability....55

The Urban Septic Field 55
Permeability Scale Effects 56
Effects of Local Geology 56
Urban Permeability Ratio Method 57
Effect of Pavements in the Waller Creek Watershed 58
CHAPTER 5: CONCLUSIONS AND FUTURE WORK 61
APPENDIX A 64
APPENDIX B 81
APPENDIX C 86
REFERENCES 103
VITA 108

List of Tables

Table 1: Measured infiltration rates of previous studies 12

Table 2: Measured infiltration from previous studies as a percentage of rainfall..... 13

Table 3: Summary of scanline characteristics..... 49

Table 4: Summary of sample point characteristics. 50

Table 5: Table of saturated hydraulic conductivities. 60

List of Figures

Figure 1: The urban rainfall recharge relationship 9

Figure 2: Plot of intial abstraction from urbanized and unurbanized watersheds. 10

Figure 3: Plot of constant loss for urbanized and unurbanized watersheds. 11

Figure 4: The study area with scanline locations. 24

Figure 5: Using double-ring infiltrometers to measure infiltration. 25

Figure 6: Experimental apparatus used to simulate joint flow. 26

Figure 7: Plot of constant head bench test data. 27

Figure 8: Plot of falling-head bench test data. 28

Figure 9: Plot of high flow 4/8 Method points. 29

Figure 10: Histogram of point hydraulic conductivities for all points. 36

Figure 11: Frequency distribution of all point hydraulic conductivities. 37

Figure 12: Histogram of all fracture and joint apertures. 38

Figure 13: Histogram of fracture apertures only. 39

Figure 14: Histogram of expansion joint apertures only. 40

Figure 15: Frequency distribution of combined fracture and joint apertures. 41

Figure 16: Frequency distribution of fracture apertures. 42

Figure 17: Frequency distribution of joint apertures. 43

Figure 18: Rose diagram of all fracture and joint trends. 44

Figure 19: Rose diagram of fracture trends. 45

Figure 20: Rose diagram of joint trends. 46

Figure 21: Equivalent hydraulic conductivities plotted against apertures 47

Figure 22: Time discharge relation for select points on scanlines 12 through 20 .. 48

Figure 23: Hyetographs of storm depth versus storm duration. 59
Figure 24: Guelph Permeameter hydraulic conductivity measurements..... 59
Figure 25: Scanline 1000 site map and summary..... 87
Figure 26: Scanline 6000 site map and summary..... 88
Figure 27: Scanline 7000 site map and summary..... 89
Figure 28: Scanline 8000 site map and summary..... 90
Figure 29: Scanline 9000 site map and summary..... 91
Figure 30: Scanline 10000 site map and summary..... 92
Figure 31: Scanline 11000 site map and summary..... 93
Figure 32: Scanline 12000 site map and summary..... 94
Figure 33: Scanline 13000 site map and summary..... 95
Figure 34: Scanline 14000 site map and summary..... 96
Figure 35: Scanline 15000 site map and summary..... 97
Figure 36: Scanline 16000 site map and summary..... 98
Figure 37: Scanline 17000 site map and summary..... 99
Figure 38: Scanline 18000 site map and summary..... 100
Figure 39: Scanline 19000 site map and summary..... 101
Figure 40: Scanline 20000 site map and summary..... 102

CHAPTER 1: INTRODUCTION

> *Because of the brevity of the period, man's work will sink into insignificance when viewed as part of geologic history. Nevertheless, during the present short chapter of that history, man's work is very important and as worthy of a place in geologic textbooks as are the actions of the sea or the rivers (Sherlock, 1922).*

Humankind's effects on the surface of the Earth are profound. If the combined effects of construction, agriculture, and mining are taken into account, the amount of material moved by humans is an estimated 40 – 45 Gt/yr (Hooke, 1994). The world's rivers, in comparison, transport approximately 24 Gt/yr. In fact, if the total amount of material moved by humans in the past 5000 years were dumped onto a pile, it would form a mountain range 4 km high, 40 km wide, and 100 km long. If current rates are maintained, the mountain range will double in length in the next 100 years (Hooke, 2000). Clearly, geoscientists will have to account for materials that have been made or moved by humans.

The most rapidly expanding of humans' effects—urbanization and the associated construction of roads, parking lots, and structures—is altering both rates of groundwater recharge and permeability distributions (Sharp *et al.*, 2003). In the United States an area roughly the size of two New York cities is urbanized every year (Sharp, 1997). Austin, Texas, the site chosen for this study, has undergone a 640-percent increase in area since 1964 (Garcia-Fresca, 2004), which does not include the explosion in growth of the surrounding communities. Of note is that these changes are occurring over a few decades, in what amounts to a geologic instant (Sharp *et al.*, 2001). A thorough understanding of the effects of urbanization is necessary to address the problems which will be faced by urban areas in the future.

EFFECTS OF URBANIZATION

As it affects the water balance, an accounting of the effects of urbanization is commonly undertaken in terms of the amount of *impervious cover* found in the study area. This is a term that describes buildings and pavements, including roads, driveways, parking lots, and sidewalks.

Urbanization has long been understood to produce a dramatic increase in impervious surface area, increasing runoff and decreasing infiltration to underlying water-bearing zones (Lerner, 1990). The corollary effects of this increase are thought to be increased flooding, introduction of non-point source contaminants to surface water and groundwater, and a decrease in precipitation-based recharge. Because of this understanding, many cities have laws that limit impervious cover.

URBAN RECHARGE

The recharge process is defined by the relationships between climate, geology, morphology, soil condition, and vegetation (DeVries and Simmers, 2002). According to Lerner, 1990, recharge—the process whereby water enters the saturated groundwater reservoir–consists of three basic types: *direct recharge*, a diffuse process which occurs directly beneath the point of impact of precipitation; *indirect recharge*, denoting precipitation that flows on the surface or within the shallow subsurface to a mappable recharge feature, usually a river; and *localized recharge*, precipitation flowing horizontally a short distance from its point of impact prior to intersecting fractures or fissures which are too numerous to be mapped. The total recharge in a city is the sum of direct, indirect, localized, and a fourth type, *artificial recharge*, which is derived from irrigation of parks and lawns as well as leakage of water mains and storm sewers (Garcia-Fresca and Sharp, 2005). Figure 1 displays the rainfall runoff relationship.

Recharge Misconceptions

The primary basis for the claim that urbanization and the requisite increase in impervious cover leads to a decrease in recharge is based in surface water balances. Researchers have concluded that because runoff volumes, measured as stream flow, have increased as areas urbanize, recharge values must, therefore, decrease. However, there is no direct evidence linking the increase in stream flow to a decrease in recharge (Lerner, 1997b). In fact, except for one documented case, recharge in urban areas has been observed to be on the rise (Garcia-Fresca, 2004). It is likely that decreases in *depression storage*-low areas where rain water accumulates and is not available as runoff, wettable surface area, and evapotranspiration account for much of the increase in stream discharge. Schueler (1994) found no statistical differences in *base flow* between urbanized and rural watersheds. Base flow is the component of stream flow derived from groundwater that sustains flow between precipitation events. If base flows are not affected by urbanization, then it is probable that recharge is not significantly affected.

Both Lerner's and Schueler's observations are reinforced by the results of the initial abstraction-constant loss model that is being developed by William Asquith at the U.S. Geological Survey (USGS), Texas Water Center. *Initial abstraction* is the amount of precipitation that is stored by the watershed prior to the onset of runoff, and *constant loss* is the difference between rainfall and runoff after the initial abstraction has been satisfied. The model is a time-distributed watershed loss model that was developed through statistical analysis of 92 USGS streamflow gaging stations in Texas. The analysis resulted in optimal values for given storms that produced modeled hydrographs that reproduced observed hydrographs. The plots of the distribution of these parameters (Figures 2 and 3) indicate that urbanization has a significant effect on initial abstraction but slight effect on constant loss. Because runoff is equivalent to rainfall less depression

storage, evapotranspiration, and infiltration, and depression storage has been satisfied by the initial abstraction, the constant loss must be due to a combination of infiltration and evapotranspiration. There is no reason to expect evapotransporation to be significantly increased by the construction of pavements. In fact, the opposite is true. Thus, it may be extrapolated that for the studied watersheds there is no measurable decrease in the infiltration rate due to an increase in urbanization and no corresponding decrease in recharge potential (Asquith and Roussel, 2007).

Rising Water Tables

Common wisdom suggests that in cities direct recharge takes place only by the percolation of precipitation in unpaved areas. If impervious cover is expanded, then presumably recharge should decrease and the water table lower proportionally. However, in almost all cases studied to date, where shallow ground water is not used as a resource, groundwater levels are rising, indicating an increase in recharge (Lerner, 2002).

Rising water tables, in the late stage of city development, are causing a variety of problems, including localized flooding of basements, decreasing load capacity and destabilization of foundations, and mobilization of contaminants (Hooker *et al*., 1999 and Lerner, 1997b). Previous attempts to account for this increase include a decrease in evapotranspiration due to the elimination of vegetative cover—this reduction in vegetative cover led to a doubling of recharge in Perth, Australia (Appleyard *et al*., 1999)–and leakage from utility pipes and urban irrigation return flows (Lerner, 1990; Garcia-Fresca *et al*., 2005).

URBAN INFILTRATION

Infiltration is the measure of the amount of precipitation that percolates beneath the land surface. It should be noted that in areas not significantly altered by humans, a large portion of precipitation that infiltrates does not continue to flow vertically

downward to the water table. It is either held in the soil or is evapotranspirated by vegetation. Only when the subsurface has been saturated to the point that the soil moisture exceeds the *field capacity*, the ability of the soil to retain moisture by capillary forces (Bear, 1972), will the water continue vertically downward under the influence of gravity.

A review of hydrogeologic literature reveals that, as it pertains to recharge, the issue of infiltration through urban pavements has largely been ignored. Among the few hydrogeologists to broach the subject, Lerner, 2002, refers to soil moisture studies and suggests that "a proportion of the impermeable area should be treated as permeable (perhaps 50%), particularly in residential areas,." but no quantitative studies were found in the literature. Expanding the search to include civil engineering transportation research, including a review of literature at the Center for Transportation Research Library at the University of Texas at Austin, failed to turn up relevant research.

Studies were finally uncovered by reviewing civil engineering literature pertaining to the design of sewer systems. The efficient design of sewer systems requires *a priori* knowledge of the relation of urban runoff to rainfall. The amount of precipitation lost to infiltration can be calculated directly from this relationship because, along with evapotranspiration and depression storage, it can be directly measured, and accounts for the difference between rainfall and runoff.

Rainfall-Runoff Relationships

Lloyd-Davies, 1906, and Kuichling, 1909, were among the first to propose methods to formulate the altered rainfall-runoff relationship due to the construction of impervious surfaces. The Lloyd-Davies method determined a runoff coefficient by taking the ratio of the paved area to the total area, and Kuichling advocated the calculation of an impermeability factor by taking the ratio between the peak rate of runoff and the mean

rate of rainfall. Subsequent experiments included direct measurement of rainfall and runoff from urban pavements and urbanized catchments; measurement of runoff from artificially irrigated pavements; direct measurement of infiltration using a drum infiltrometer on a brick and concrete pavement; and a series of soil moisture measurements underneath urban pavements. The rainfall-runoff water balance is:

$$\text{runoff} = \text{rainfall} - \text{depression storage} - \text{evapotranspiration} - \text{infiltration} \qquad (1)$$

Tables 1 and 2 summarize the results of the previous infiltration studies, with the results of this study included for comparison. Table 1 lists the observed infiltration rates, which range from 1.8 mm/h to as high as 27 mm/h; Table 2 summarizes the observed percentage of precipitation that infiltrates urban pavements and urbanized areas, indicating that from 6 to 41.6 percent infiltrates. These data indicate that infiltration is among the most important aspects in the rainfall-runoff relation for urban pavements. When sewer systems were designed under the assumption that pavements were impervious, “Authorities noted that sewers rarely seemed to operate at anything approaching their full capacities” (Watkins, 1962); and Hollis and Ovenden, 1988b, were amazed when water applied to a curb in their study area at a rate of 18.67 l/min failed to reach the drain.

In addition to estimates of infiltration, many of these studies provide estimates of the other parameters of the rainfall-runoff water balance. Depression storage as depth of rainfall ranges from 0.4 mm to 1.23 mm (Hollis and Ovenden, 1988a), and as a percentage of rainfall ranges from 26 to 31 percent. Evapotranspiration as a percentage of rainfall ranged from 18 to 21 percent by Davies and Hollis, 1981 and Colyer, 1983, but

was found to be an order of magnitude less significant than infiltration in a subsequent study (Hollis and Ovenden, 1988b).

It may be concluded that these reductions in runoff are a true reflection of the hydrologic characteristics of the pavement (Hollis and Ovenden, 1988a, and Lerner, 2002) and that extremely low runoff is attributable to infiltration (Colyer, 1983). The mechanism for this infiltration has only been studied indirectly and is presumed to consist of seepage through fractures and through joints between pavement blocks (Davies and Hollis, 1981; Hollis and Ovenden, 1988a; Kidd, 1978; Pratt and Henderson, 1981), which form preferential flow paths and an avenue for localized recharge.

PREFERENTIAL FLOW PATHS

It has been observed that changes in the flow paths for precipitation and an increase in preferential flow paths in urban areas can result in an increase in recharge when compared to rural areas (Lerner, 1997b). Preferential flow paths "short circuit" the path to the water table (Stephens, 1994). In the urban environment it is critical to identify these conduits because they significantly reduce both transport time through the unsaturated zone (Scanlon *et al*, 2002) and subsequent estimation of recharge (Lerner, 1990 and Simmers, 1998).

Fracture Flow

In parallel plate models, fractures have been shown to have discharges and hydraulic conductivities in proportion to the cubes and the squares of their apertures, respectively. Due to these enormous effects on permeability, fractures have been studied intensely. They are recognized as the most important source of hydraulic conductivity in plutonic rocks, volcanic rocks, some carbonate rocks, and mud rocks (Marrett, 1996). This is also the case for urban pavements, where they provide the obvious and, in most cases, only preferential pathways for infiltration. Most urban pavements can be viewed as

purely fractured media–rock in which fractures provide all of the hydraulic conductivity and account for all of the storativity (Sharp, 1993).

Generally speaking, the more open fractures that are present, the more permeable a rock formation. The critical components of fractured media characterization include fracture orientation, frequency, aperture, length, and interconnectivity, as well as an understanding of the distribution of these attributes. These aggregate properties of individual fracture characteristics can ultimately be generalized with scaling relations. Although fracture characteristics are three dimensional, most data sets are collected along one-dimensional scanlines, and in localities with sub-vertical fractures this method has proven to be sufficient to sample fracture populations (Marrett, 1996).

PURPOSE AND SCOPE OF WORK

Research in the area of urban recharge has been largely neglected, and few case studies addressing pavement permeability have been reported in the literature (Lerner, 2002). Accurate hydrogeological data and valid interpretations for urban areas are critical to preserve water quality, manage aquifers, and to allow for the development of conjunctive use strategies for additional urban recharge (Sharp, 1997).

This study proposes to refute the assumption that urban pavements are impervious, to show that fractures and joints have sufficient permeability to have an impact on localized recharge, and to provide data that help define the aggregate characteristics of these pavements. Data about location, infiltration rate, aperture, trend, pavement type, and fracture type are reported and analyzed to determine the flow properties of urban pavements. These properties are then qualitatively analyzed to determine their overall effect on urban recharge.

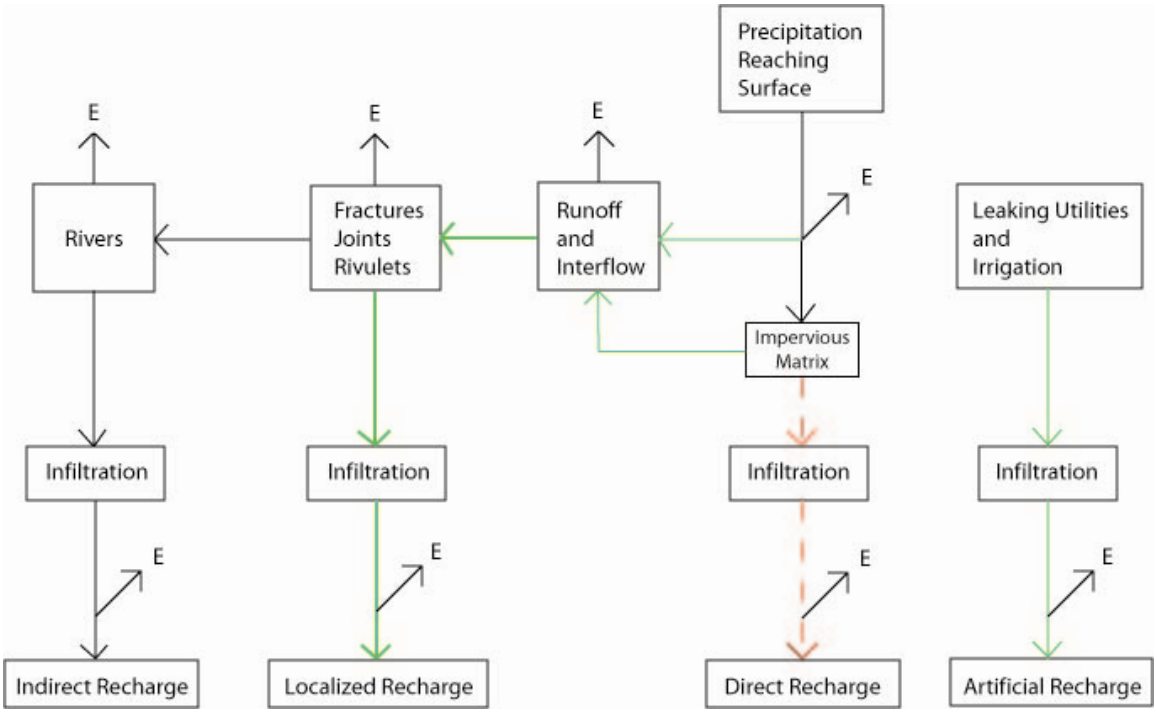

Figure 1: The urban rainfall recharge relationship. Evapotranspiration is indicated by E. (Modified from Lerner, 1997a)

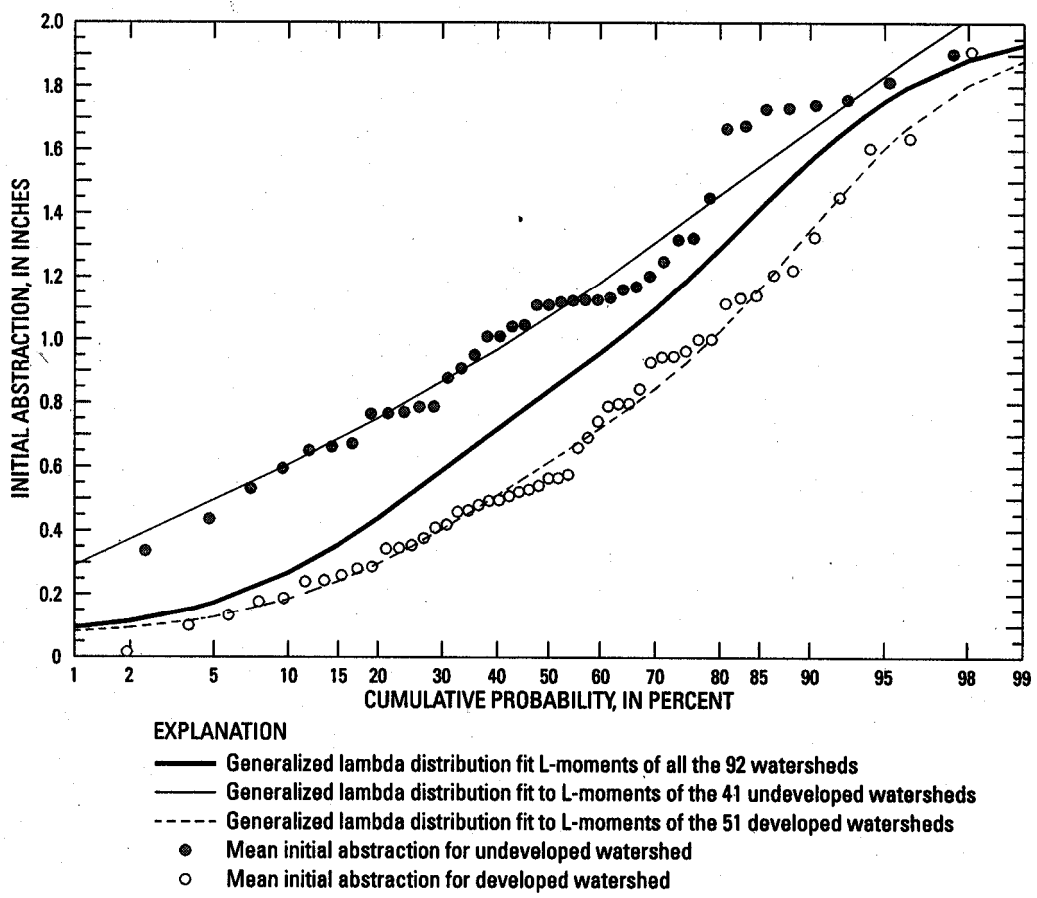

Figure 2: Plot of intial abstraction from urbanized and unurbanized watersheds in Texas (Source: Asquith and Roussel, 2007).

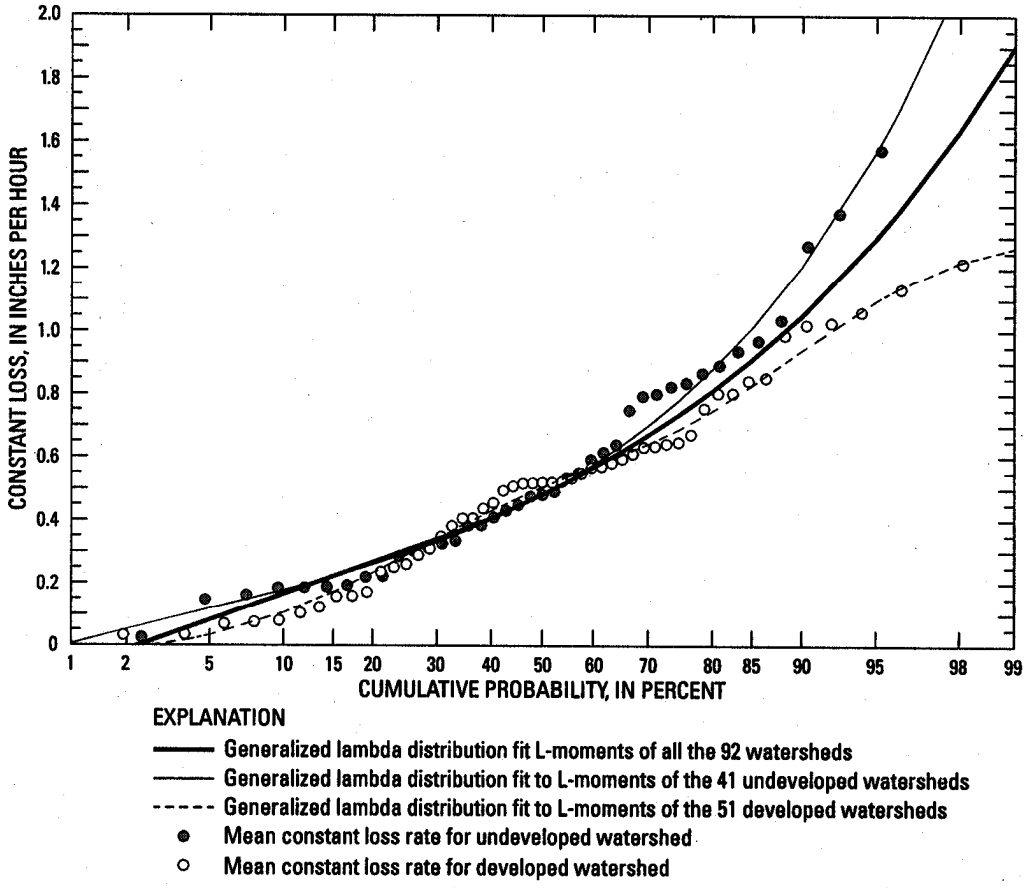

Figure 3: Plot of constant loss for urbanized and unurbanized watersheds in Texas (Source: Asquith and Roussel, 2007).

Table 1: Measured infiltration rates of previous studies. This study is included for comparison.

Author	Year	Infiltration Rate	Pavement Type	Method
Appleby	1937	1.8 mm/h	urban pavement	Unkown
Zondervan	1978	7 - 27 mm/h	concrete road	pavement irrigation
van Dam and van de Ven	1984	7.4 mm/h	brick and concrete	drum infiltrometer
Pratt and Henderson	1981	0.75 ml/sec/meter	concrete curb	pavement irrigation
Hollis and Ovenden	1988	14.25 - 46.28 l/min	asphalt road	pavement irrigation
This Study	2007	2.1 mm/h	urban pavement	ring infiltrometer

Table 2: Measured infiltration from previous studies as a percentage of rainfall. This study is included for comparison. The Hollis and Ovenden infiltration is modified by Colyer's estimates of initial abstraction and evaporation.

Author	Year	Infiltration %	Pavement Type	Method
Watkins	1962	21	asphalt road	direct measurement
Falk and Niemczynowicz	1978	7.4-17	asphalt catchments	direct measurement
Davies and Hollis	1981	34	asphalt road	direct measurement
Colyer	1983	36	asphalt road	direct measurement
Hollis and Ovenden	1988	24.7 - 41.6	asphalt road	direct measurement
Stephenson	1994	22	urbanized catchment	direct measurement
Lee and Heaney	2003	30	urbanized catchment	direct measurement
Ragab *et al.*	2003	6 - 9	asphalt roads	soil moisture balance
This Study	2007	21	urban pavement	ring infiltrometer

CHAPTER 2: METHODS

This study necessitated the development of new methods to quantify pavement permeability. Data collection, analysis, and method refinement were conducted in four phases, the first three of which produced half of the data set; the final phase produced the second half. Though the initial methods employed to collect the data were time consuming and subsequently modified, data gathered from them remain valid.

LOCATION AND HYDROGEOLOGIC SETTING

All of the data for this experiment were collected on pavements roughly contained within the Waller Creek Watershed in Austin, Texas. The scanline locations within the watershed are indicated on Figure 4. This small watershed possessed these desirable characteristics: convenience, since it both crosses the campus of The University of Texas at Austin (UT) and, farther north, contains the home of the author; hydrogeological importance, consisting primarily of Quaternary alluvial deposits, which have been determined to produce the bulk of recharge within the city (Garcia-Fresca, 2004); complete urbanization, which is by definition the basic qualification needed for this study; and significance, in that it is a subject of interest to other hydrogeologists at UT. It is anticipated that the data developed in this thesis will contribute to a greater understanding of the urban effects on this and other watersheds.

Geology

The surface geology in the watershed is dominated by a thin layer of Colorado River alluvial deposits, predominantly fine-grained over-bank deposits that were deposited unconformably on the Cretaceous Austin Chalk Formation. These types of deposits typically have significant hydraulic conductivity but are known to normally have

two orders of magnitude lower vertical hydraulic conductivity than horizontal hydraulic conductivity.

Land Use

Land use in the northern half of the watershed is composed primarily of single-family and multifamily dwellings, with some mixed commercial space. The southern half of the watershed is dominated by mixed commercial and office space (Garcia-Fresca, 2004). This study was completed in the northern half of the watershed, from the middle of the UT campus to State Highway 183.

Individual Site Selection

The goal of this study is to quantify the permeability of typical pavements within the Waller Creek Watershed. In order to get a representative sample of different ages of pavement, the locations were selected at relatively even intervals from Highway 183 south to the UT campus with the idea that the farther north one travels from campus, the younger the pavements are likely to be. Information on the age and repair history of the pavements was sought from the City of Austin, but could not be obtained.

The individual scanline locations were selected on the basis of pavement type, safety, and whether or not they were representative of area pavements. The first half of the study focused on collecting data from a variety of parking lots, roads, and concrete curb gutters. The second half of the study focused on the concrete curb gutters only, because they receive the largest portion of storm flow. As a safety precaution and practical consideration, sites with low traffic flow were preferred. Additionally, visual criteria were used to confirm that each selected site was representative of the pavements in the vicinity. Specific data on location and characteristics of the different sites is presented in Appendix C.

Simplifying Assumption

A Darcy's Law solution was employed to calculate the equivalent hydraulic conductivity for each sample location which is a measure of fracture and expansion joint *permeability*, the ease with which water flows through an area. The equivalent hydraulic conductivity relates the infiltration rate due to the fracture or joint to the effective area of the inner-ring of the double-ring infiltrometer in terms of the hydraulic conductivity of a porous media. Darcy's Law relates discharge Q [L^3/t] to hydraulic conductivity K [L/t], area A [L^2], and the hydraulic gradient i [L/L], which is the change in head pressure over a length or distance.

$$Q = KiA \tag{2}$$

For vertical flow this change in head is proportional to the change in distance, and in saturated media if there is negligible pressure head from surface ponding, then it is reasonable to assume that the hydraulic gradient is one.

The infiltration rate I [L/t] is equal to the discharge divided by the cross-sectional area. It follows that for vertical flow the infiltration rate is equal to the hydraulic conductivity. All phases of analysis are based on this assumption.

$$I = Q / A = K \tag{3}$$

PHASE I – PROOF OF CONCEPT AND METHODS DEVELOPMENT

The first phase of the method development was conducted on the asphalt and concrete parking lot located immediately east of the geology building on the UT main campus. This study, titled "Fracture Permeability in Urban Pavements," is included as Appendix A.

Initial Experiment Location

Three criteria were used to select the location for this experiment. The first was the necessity of a location with a sufficient amount and variety of fractures and expansion

joints to sample. The second was the need to sample at least two pavement types, in this case asphalt and concrete. The last was proximity. The parking lot located just outside the east basement door of the Jackson School of Geosciences building at the University of Texas at Austin met these criteria.

Initial Experiment Design

The goal of the experiment was to determine the hydraulic conductivity of pavements due to fractures and expansion joints. In order to sample the pavement with minimal bias, a 100-foot scanline was set up oriented approximately north-south, intersecting various types of expansion joints and fractures on both asphalt and concrete portions of the parking lot. Infiltration tests were conducted at each point that a fracture or joint intersected the scanline, as well as in adjacent unfractured areas of the different pavements. The cumulative infiltration rate or discharge could then be compared to the area of pavement represented by the scanline to determine the equivalent fracture permeability.

Initial Experiment Apparatus

A double-ring infiltrometer (Figure 5) was sealed to the pavement with Oatey Plumber's Putty. The double-ring configuration was necessary to prevent lateral flow in the fractures. Once the infiltrometer was sealed to the ground, the outer ring was filled with water to ensure that there was no leakage into the inner ring. This ensured that water would not leak through the seal into the outer ring, skewing the infiltration rate calculation. Once it was determined that there was no communication between the rings, both rings were filled to a depth of approximately six centimeters (an arbitrary water depth representing a level that was convenient to work with). After each infiltration test was conducted, measurements of the fracture length and average aperture of the fracture or joint were measured using a scale or the fracture comparator designed by Dr. Orlando

Ortega and Dr. Randall Marrett of the Fracture Research and Application Consortium at UT.

A Guelph Permeameter was used as a constant-head device to maintain 6 cm of water in the inner ring of the infiltrometer. The level in the outer ring was kept at the same level as the inner ring by adding water manually. Measurements from the Guelph were recorded at even intervals during the experiments to determine the flux through the double ring. This configuration worked well at high flow rates. It was observed, however, that at very low flow rates the Guelph was unreliable. For each of the remaining sample locations a falling-head test was conducted first. If the flow rate was determined to be sufficient, then the Guelph was employed to conduct a constant-head test; if not, then only the initial falling-head data were recorded. After the constant head test, a final falling-head test was conducted for comparison to the first.

Initial Experiment Data Collection

The data were collected at each sample location by measuring the height of the water column at the beginning of the test-with a clear plastic scale with millimeter divisions, and at succeeding increments of time-measured with a digital stop watch, until the rate of change had stabilized. Water height was measured using a millimeter-ruled scale in the infiltrometer for the falling head tests, and using the internal millimeter graduations in the large ring of the Guelph Permeameter for the constant head tests. These changes in height of the water column were then converted to volumes based on the change in volume per unit height of the different devices.

Initial Method Problems and Refinement

The data collected during the first phase are considered reliable, but three problems with the method were determined. First, the use of the Guelph Permeameter as a constant head device was applicable only on fractures with the largest hydraulic

conductivities. Consistency required either reliance on falling head data alone or a more precise method of maintaining constant head. Second, the method failed to account for the change in infiltration rate due to a drop in pressure head as the ponding depth in the double-ring infiltrometer dropped. Finally, the method took too much time to allow collection of large amounts of data.

PHASE II – BENCH TESTING

During a storm, the ponding depth of water on a pavement will vary primarily as a function of rainfall intensity and pavement slope. Because these effects are so variable, and because of a desire to adopt a conservative approach, a simplifying assumption was made that ponding depths are zero. Therefore, a method to account for the effects of ponding depth was needed.

The driving forces behind infiltration rate are pressure head and gravity. Theoretically, the pressure head due to ponding depth should decrease proportional to a decrease in the height of the water column in the double-ring infiltrometer. When the depth over the pavement reaches zero, gravity should be the only force driving infiltration. A model of a simple pavement joint over a well-drained porous media was constructed to test this relationship and to demonstrate the general validity of a simple falling-head method that could be applied to all locations regardless of infiltration rate. The data for the bench tests are included as Appendix B.

Bench-Testing Apparatus

The experimental apparatus, shown in Figure 6, consisted of a plywood box partially filled with porous media (pea gravel or very coarse sand), with two concrete pave stones placed directly on top of the porous media. The gap between the concrete pave stones was meant to simulate a joint in concrete pavement and a double-ring infiltrometer was sealed to the simulated pavement surface using Oatey Plumber's Putty.

Three constant-head and three falling-head experiments measured the volume of water that infiltrated the joint over a given time for a given height of water in the inner-ring. The aperture of the joint, the sub-grade, and the water depth in the infiltrometer were varied to determine their effects on infiltration rates.

Bench Test Results and Method Refinement

Figures 7 and 8 display the results of the bench test. They clearly demonstrate the linear relationship between ponding depth and discharge. In addition, the results from the constant head analysis are sufficiently similar to the results from the falling head analysis to justify a simplified falling-head methodology.

PHASE III – 4/8 METHOD

The 4/8 method was developed to take advantage of the linear relationships observed during bench testing and was used to collect and analyze data from scanlines 6 through 11. In this method, the double-ring infiltrometer was sealed to the pavement at each point where a 30-meter scanline intersected a fracture or joint, in the same way as in the initial method. Additionally, the fracture and joint trends were measured with a Bunton Pocket Transit for further analysis.

4/8 Method Data Collection

In this method the inner-ring of the infiltrometer was filled to a depth of 8 cm and observed to determine that there was no significant connectivity between the inner and outer rings. The outer-ring was then filled to the same depth and the apparatus was allowed to equilibrate for 5 minutes. It was recognized during the initial experiments, and confirmed by subsequent data, that infiltration rates generally decrease within the first five minutes of infiltration. Zondervan (1978) noted this leveling out of infiltration rate after 7 minutes in his road irrigation experiments. It is presumed that this effect is the

result of the filling of void space and the transition from unsaturated to saturated conditions in the road subgrade.

After 5 minutes, the change in depth of water in the inner-ring was recorded over a time period appropriate for the observed flow rate, these time periods ranged from 20 seconds to 5 minutes, and generally limited so that the drop in the water level did not exceed 2 cm. This process was repeated twice, first for an initial depth of 8 cm, then for an initial depth of 4 cm, removing the water from both inner and outer rings between the two processes.

4/8 Method Data Analysis

An average ponding depth was calculated for each initial depth by taking the average of the beginning depth and the final depth after the prescribed time period. The infiltrated volume IV [L^3] of water was determined by multiplying the difference in depth [L] by the area of the inner ring A_{ir} [L^2].

$$IV = \Delta d \times A_{ir} \tag{4}$$

$$Q = IV / \Delta t \tag{5}$$

The infiltrated volume was then divided by the time period Δt [t] to determine the discharge rate Q [L^3/t]. These values were converted to equivalent hydraulic conductivity K [L/t] by dividing by the area of pavement A_{pv} [L^2] sampled; this area is less than the area of the inner ring due to the presence of the Plumber's Putty sealing ring.

$$K = Q / A_{pv} \tag{6}$$

The point equivalent hydraulic conductivity K_0 [L/t] was then calculated by linear extrapolation through the plots of hydraulic conductivity versus average depth to a ponding depth of 0 cm.

Finally, the scanline equivalent hydraulic conductivity was calculated by multiplying the point hydraulic conductivity by the area of the inner ring to get back to

discharge [L^3/t] for each point, taking the sum of all the points on the scanline, and dividing by the effective width of the inner ring W_e [L] times the scanline length L_t [L], which is the area represented by the scanline.

$$Keq = (\Sigma K_0 A_{pv}) / W_e L_t \quad (7)$$

4/8 Method Problems and Refinement

The 4/8 Method allowed for more efficient collection, of data, but after attempting to use it to calculate equivalent hydraulic conductivity for 6 scanlines, two observations necessitated the development of an alternative method. The first was that for each sampling interval relatively minor measurement errors had too much influence on the slope of the line fitted to the average ponding depth versus hydraulic conductivity. The result was that for approximately 30 percent of the points with infiltration rates in excess of 0.1 cm/min, the hydraulic conductivity was observed to be near zero or negative. Not only was this counter intuitive, but because there was never an instance in which infiltration was observed to reverse itself with water flowing back out of the fracture, these analyses were clearly erroneous.

The second observation was that, in most cases, the infiltration at a starting depth of 8 cm for a given time step was approximately twice that of the subsequently measured 4-cm infiltration. These data, plotted as infiltration in centimeters versus ponding depth in Figure 9, were the basis for the final and most basic sampling and analysis method.

PHASE IV – THE WILES RATIONAL METHOD

The Wiles Rational Method was used to re-analyze data from scanlines 6 through 11 and to collect and analyze data from scanlines 12 through 20. The method is simple; the results are reasonable; and it allows for the efficient collection of large amounts of data. Data from scanline 1 were not collected in a manner that allowed for their reanalysis using this method.

Method Rationale

Using the data for the points with the 30 highest infiltration rates from scanlines 6 through 11, the average ratio of infiltration at 4 cm initial depth to 8 cm initial depth was determined be 0.59 or approximately 60 percent with a standard deviation of 11 percent. A similar average ratio was calculated from the bench test data to be 0.75. The ratios of the field data points were deemed to be both the most conservative and most appropriate for use in extrapolating data. By linear extrapolation to a ponding depth of 0 cm, the ratio was calculated to be 0.174 or 17.4 percent of the value at 8 cm initial ponding depth ± 22 percent.

Rational Method Data Collection

Data were collected in the same manner as the 4/8 Method. However, there was no need to collect data for an initial ponding depth of 4 cm. In addition, starting with scanline 12 and continuing through scanline 20, time-distributed infiltration data were collected from the first fracture or joint that had a minimum infiltration rate of 0.20 cm/min. These data record the change in infiltration rate with time and were collected by observing the infiltration for an initial ponding depth of 8 cm for a given time period; then refilling the double-ring infiltrometer and repeating the process until the infiltration rate was observed to stabilize.

Rational Method Data Analysis

All of the data from scanline 6 through scanline 20 were reanalyzed using the rational method. The 8-cm point equivalent hydraulic conductivities and the total scanline equivalent hydraulic conductivities were calculated in the same way as the 4/8 method. The only difference was that the 0-cm point hydraulic conductivity was simply calculated to be 17.4 percent of the 8-cm point hydraulic conductivity.

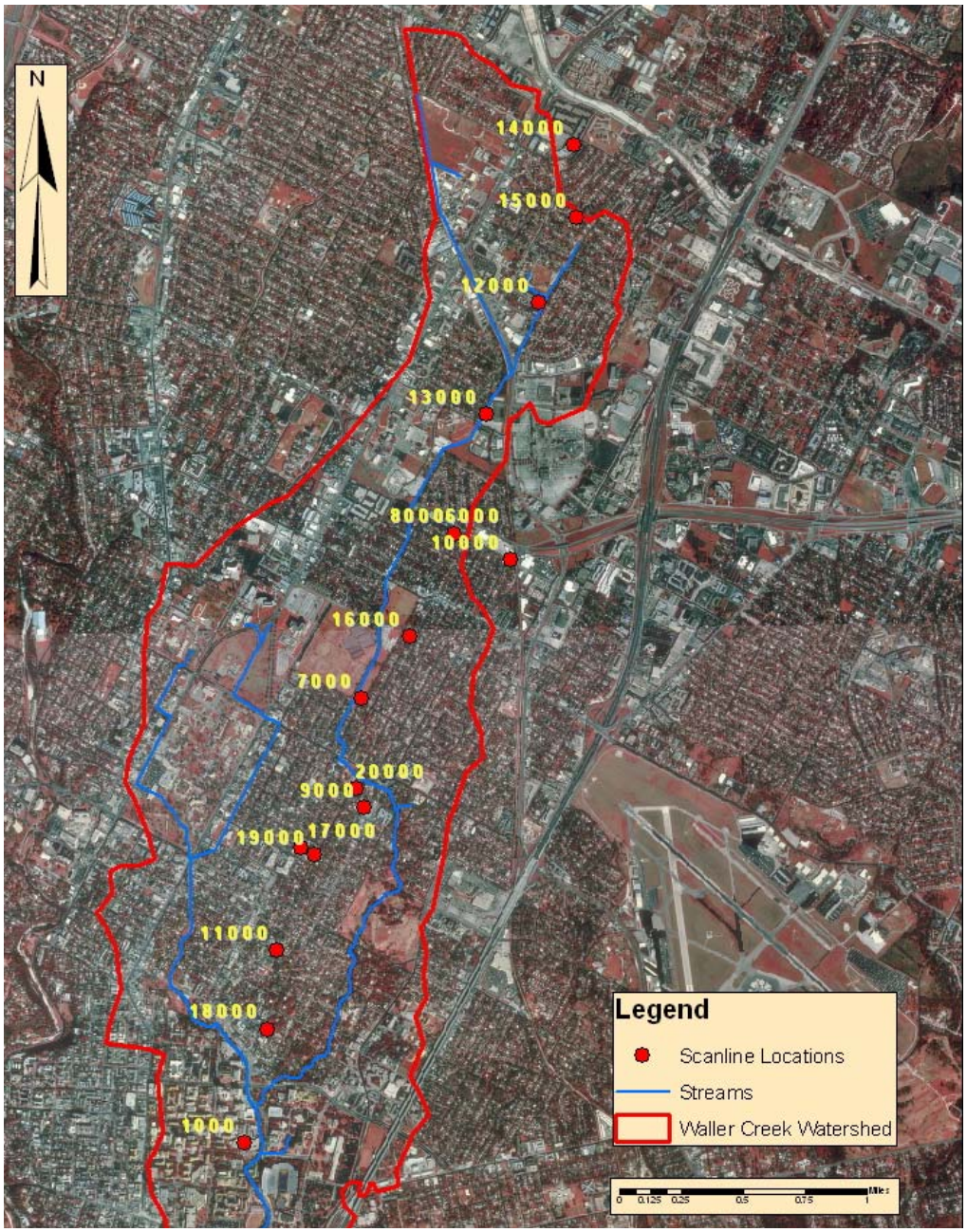

Figure 4: The study area with scanline locations.

Figure 5: Using double-ring infiltrometers to measure infiltration for fractures and joints crossed by scanline 1.

Figure 6: Experimental apparatus used to simulate joint flow over well drained porous media.

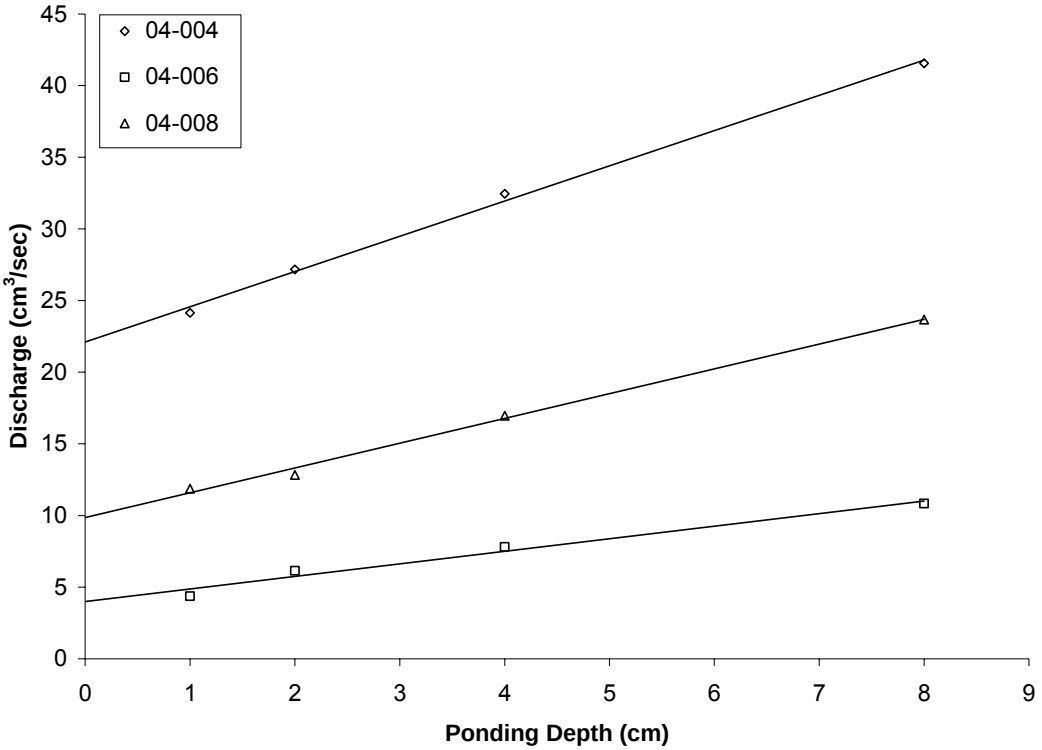

Figure 7: Plot of constant head bench test data for sample points 04-004 (0.25 mm aperture and pea gravel subgrade), 04-006 (0.1mm aperture and pea gravel subgrade), and 04-008 (0.1 mm aperture and coarse sand subgrade).

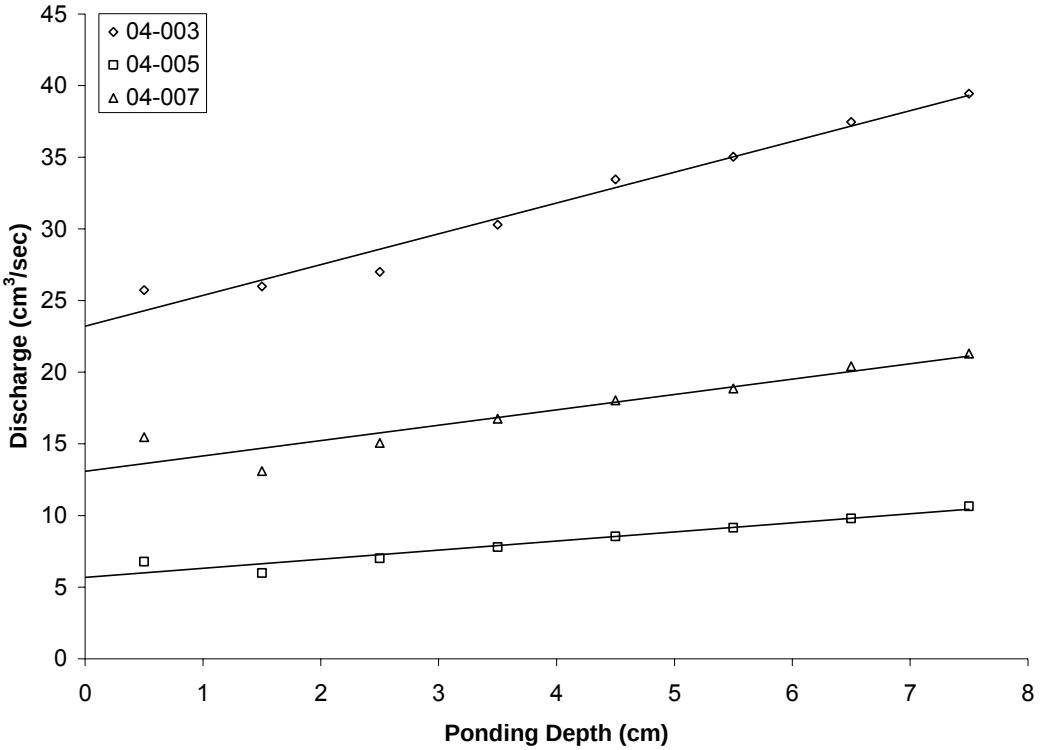

Figure 8: Plot of falling-head bench test data for sample points 04-003 (0.25 mm aperture and pea gravel subgrade), 04-005 (0.1mm aperture and pea gravel subgrade), and 04-007 (0.1 mm aperture and coarse sand subgrade). The data points at ponding depth 0.5 are most likely in error due to the difficulty in collecting data at such a shallow depth.

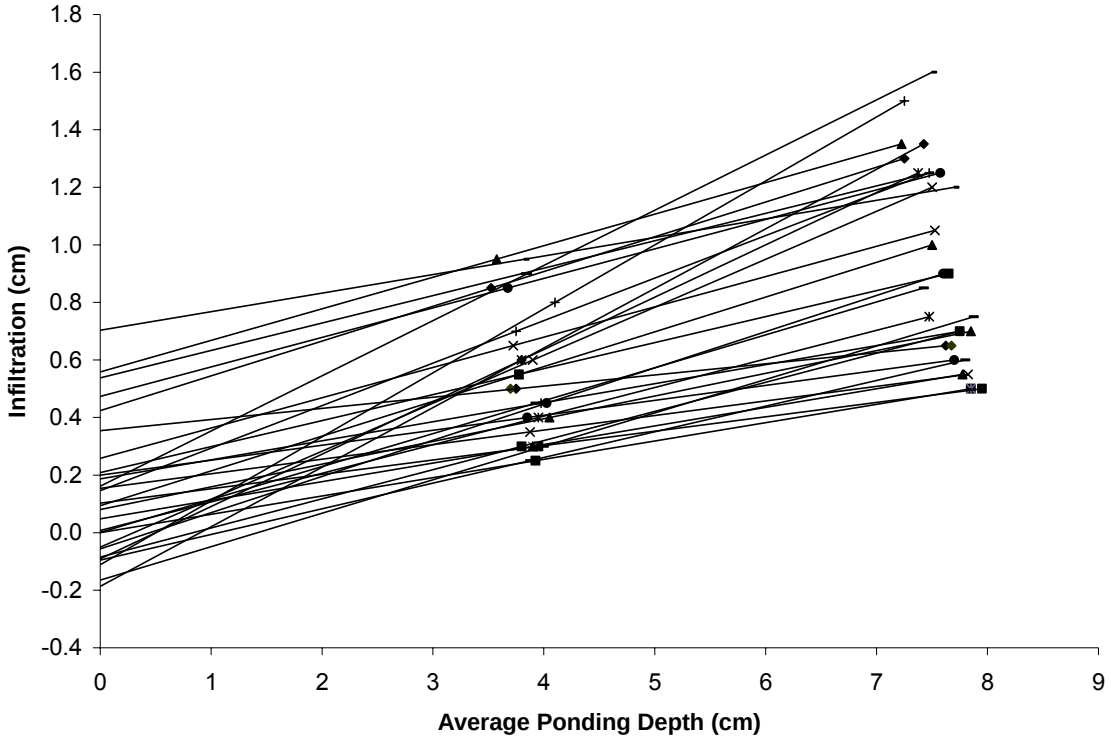

Figure 9: Plot of high flow 4/8 Method points with trend lines illustrating y-intercepts. Note that some of the highest flows have some of the lowest intercepts.

CHAPTER 3: RESULTS

HYDROGEOLOGIC SUMMARY OF SCANLINES

A total of 16 scanlines were completed on 5 pavement types: 7 concrete curb gutter sections, 3 asphalt roads, 2.5 asphalt parking lots, 2.5 concrete parking lots, and 1 concrete road. The pavement types and the condition of the pavements were observed to be typical of those found throughout the northern half of the Waller Creek Watershed. The individual scanline attributes are summarized in Table 3, and all scanline data tables are included as Appendix C.

Present at each scanline location was at least one permeable fracture or joint that provided an avenue for infiltration. The equivalent hydraulic conductivities were found to range from $4.1 \cdot 10^{-4}$ cm/s to $2.6 \cdot 10^{-6}$ cm/s for all of the pavement types; from $4.1 \cdot 10^{-4}$ cm/s to $3.2 \cdot 10^{-6}$ cm/s for the concrete curb gutters; from $2.9 \cdot 10^{-5}$ cm/s to $1.2 \cdot 10^{-5}$ cm/s for the asphalt roads; from $7.1 \cdot 10^{-5}$ cm/s to $3.7 \cdot 10^{-5}$ cm/s for the asphalt parking lots; and from $1.1 \cdot 10^{-4}$ cm/s to $8.5 \cdot 10^{-5}$ cm/s for concrete parking lots. The lone concrete road sampled had the lowest, $2.6 \cdot 10^{-6}$ cm/s, equivalent hydraulic conductivity of all of the points. It should be noted that purely concrete roads are extremely rare within the watershed and that the value determined for the single road sampled is likely to be anomalously low based on flow rates observed in concrete curb gutters and concrete parking lots.

HYDOGEOLOGIC SUMMARY OF POINT DATA

A total of 200 point locations were sampled; 197 were either a joint or a fracture, and 3 were intact pavement sections. Apertures were measured to range from 0.05 mm to 25 mm; for those points with measurable infiltration, the point equivalent hydraulic conductivities ranged from $3.98 \cdot 10^{-5}$cm/s to $6.68 \cdot 10^{-2}$ cm/s respectively. Approximately 33 percent of the locations had no measurable infiltration.

A data summary is presented in Table 4. The point data are presented by pavement type—either asphalt or concrete—and further subdivided as fractures, expansion joints, multi-fractures, or intact. Multi-fractures are locations at which more than one fracture was contained within the footprint of the inner ring of the infiltrometer; intact sample points are locations where the surface within the inner ring of the infiltrometer appeared to lack fractures or joints. Three intact locations were sampled to confirm that matrix infiltration was effectively zero, and subsequent zero-infiltration readings at fracture or joint locations indicated that the sampling of intact locations would be redundant.

Asphalt Pavements

Of the 200 points sampled, 59 were located on asphalt pavements. Of these, 36 percent had no measurable infiltration using the double ring technique. Fractures were the dominant pathway for infiltration, with equivalent hydraulic conductivities ranging from $2.12 \cdot 10^{-3}$ cm/s to $7.95 \cdot 10^{-5}$ cm/s. The asphalt fracture apertures ranged from 0.1 mm to 10 mm. Joints between two sections of asphalt pavement are rare in the study area, and only two were sampled.

Concrete Pavements

Due to the emphasis on concrete curb gutters, the majority of the points were collected on concrete pavements. A total of 121 points were collected on concrete pavements. Of these, 36 percent had no measurable infiltration; this was identical to the measurements taken on asphalt pavements. Fractures were the most common avenue of infiltration and were observed to have the highest infiltration rates. Expansion joints were about 50-percent less common, but had a significant effect on infiltration as well. The equivalent hydraulic conductivities for concrete pavements ranged from $6.68 \cdot 10^{-2}$ cm/s to $3.98 \cdot 10^{-5}$ cm/s for fractures and from $6.56 \cdot 10^{-3}$ cm/s to $7.95 \cdot 10^{-5}$ cm/s for joints.

Apertures ranged from 0.25 mm to 9.0 mm for fractures and from 0.05 mm to 20.0 mm for joints. Though the apertures for expansion joints are much larger than fractures, their effect on infiltration is diminished due to the fact that they are commonly filled with either form lumber or asphalt sealant.

Combination Pavements

Combination pavements are those at the transition from asphalt to concrete pavement. This is the typical case on roads and parking lots in Austin, where asphalt pavements transition to concrete curb gutters. The point of this transition is necessarily classified as a joint. While combination pavements represent only 5 percent of the data points, only one of the points failed to demonstrate measurable infiltration, leading to the judgment that these types of pavements contribute significantly to scanline equivalent hydraulic conductivity. Of the six asphalt pavements sampled only one, scanline 07000, failed to have at least one combination pavement contributing to infiltration. The equivalent hydraulic conductivity calculated for these points ranged from $6.76 \cdot 10^{-3}$ cm/s to $3.98 \cdot 10^{-5}$ cm/s for apertures that ranged from 0.10 mm to 25.0 mm.

HYDROGEOLOGIC SUMMARY OF CUMULATIVE SCANLINE DATA

The average equivalent hydraulic conductivity of the pavements studied is $5.9 \cdot 10^{-5}$ cm/s $\pm$ $1.3 \cdot 10^{-5}$ cm/s. This value was determined by summing the discharge of all of the data points and dividing by the area represented by the sum of the individual scanline areas. The equivalent hydraulic conductivity can be directly converted to an infiltration rate of 2.1 mm/h by unit conversion and can lead to a large flux of potential recharge through these supposedly impervious pavements. This figure is significant in light of the fact that the mean rainfall intensity for Austin is approximately 2.0 mm/h.

Further analysis indicated that the total pavement hydraulic conductivity is dominated by the highest-point hydraulic conductivities. The point with the single

highest-point hydraulic conductivity accounts for 33 percent; the ten highest points account for 58 percent; and the top 20 points account for 72 percent of the total equivalent hydraulic conductivity. This distribution of hydraulic conductivity necessitates the cumulative method described above to determine the pavement hydraulic conductivity, as individual scanlines are likely to over sample or under sample these highly conductive fractures and joints.

POINT HYDRAULIC CONDUCTIVITY DISTRIBUTION

Figures 10 and 11 are plots of the histogram and the frequency distribution of the point hydraulic conductivities respectively. A logarithmic distribution of data is evident in both figures. The frequency distribution begins at 33 percent because that percentage of the points had no measurable infiltration.

ATTRIBUTES OF FRACTURE AND JOINT POPULATION

Histograms

Figures 12 through 14 are histograms of all fracture and joint apertures. Figure 12 is a histogram of all fracture and joint apertures combined and appears to show a logarithmic distribution except for a slight bulge in the tail. Figure 13 is the histogram of fracture apertures only and has a similar distribution. Figure 14 is the histogram of joint apertures only and is bimodal, which accounts for the bulge observed in Figure 12.

The bimodal distribution in Figure 14 is due to a fundamental difference in the types of expansion joints sampled. The joints were observed to either be open and filled with some type of form lumber accounting for the large aperture joints, or closed, with generally only a slight gap between the adjoining sections of pavements. The logarithmic distribution of the fractures defies a simple explanation, but fracture sets in rock formations are observed to organize into both power law and log normal distributions, presumably from having formed as a result of the same stress field (Marrett, 1996). It

might be the case that fractures in urban pavements organize by virtue of a similar process, forming largely in response to “urban tectonic” down-warping of the pavements due to uneven traffic distribution.

Frequency Distributions

Figures 15 through 17 display the frequency distribution for all fractures and joints, fractures only, and joints only. These data show clear logarithmic frequency distributions which might allow for attribute prediction in similar pavements.

Fracture and Joint Trends

Figures 18 through 20 display trend data collected for all of the fractures and joints sampled. The trends show prominent NNE/SSW and WNW/ESE alignment and should be considered bi-directional. The explanation of these trends can be found in Figure 4, which shows that the streets in Austin are aligned in the same way. The map views on figures 28, 30, and 35 in Appendix C demonstrate that scanlines were oriented to intersect the dominant fracture directions and not to the pavement orientation. It may be concluded then, that fractures in these pavements form in an either sub-parallel or sub-perpendicular manner to the orientation of the trend of the road and may provide a significant anisotropy to shallow horizontal interflow.

EFFECT OF APERTURE ON EQUIVALENT HYDRAULIC CONDUCTIVITY

The realization that the equivalent hydraulic conductivity and apertures are similarly distributed leads to the hypothesis that they are related. However, as demonstrated in Figure 21, there seemed to be no correlation between hydraulic conductivity and aperture for either fractures or joints in either asphalt or concrete pavements. This fact, while discouraging, at least demonstrates that the sizes of fractures and joints in pavements is not the fluid-flow rate-limiting step and must have an

equivalent hydraulic conductivity at least as high as $5.9 \cdot 10^{-5}$ cm/s, and likely much higher.

TIME DISCHARGE RELATION

For the last 9 scanlines, the first point with an initial infiltration rate in excess of 0.2 cm/min was further sampled to determine the change in infiltration rate with time. These data are presented in Figure 22 as point discharge in (cm^3/s) versus elapsed time. These data show that discharge generally levels out and becomes constant after 400 to 600 seconds, but this effect should not be considered conclusive.

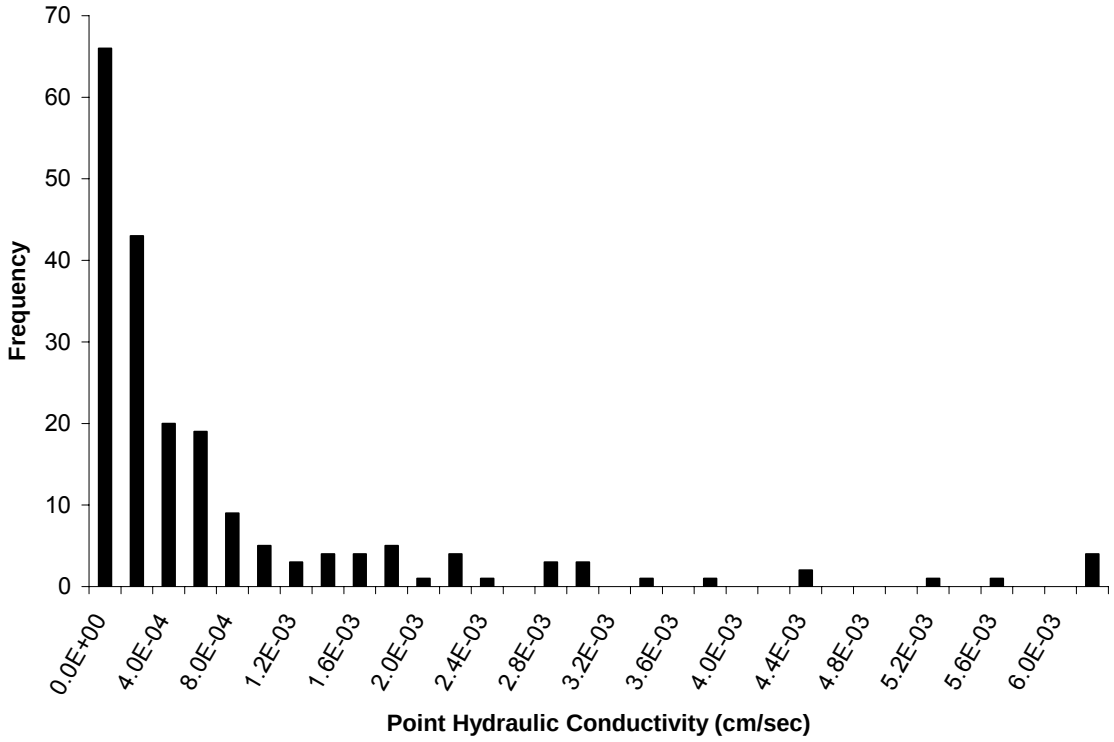

Figure 10: Histogram of point hydraulic conductivities for all points.

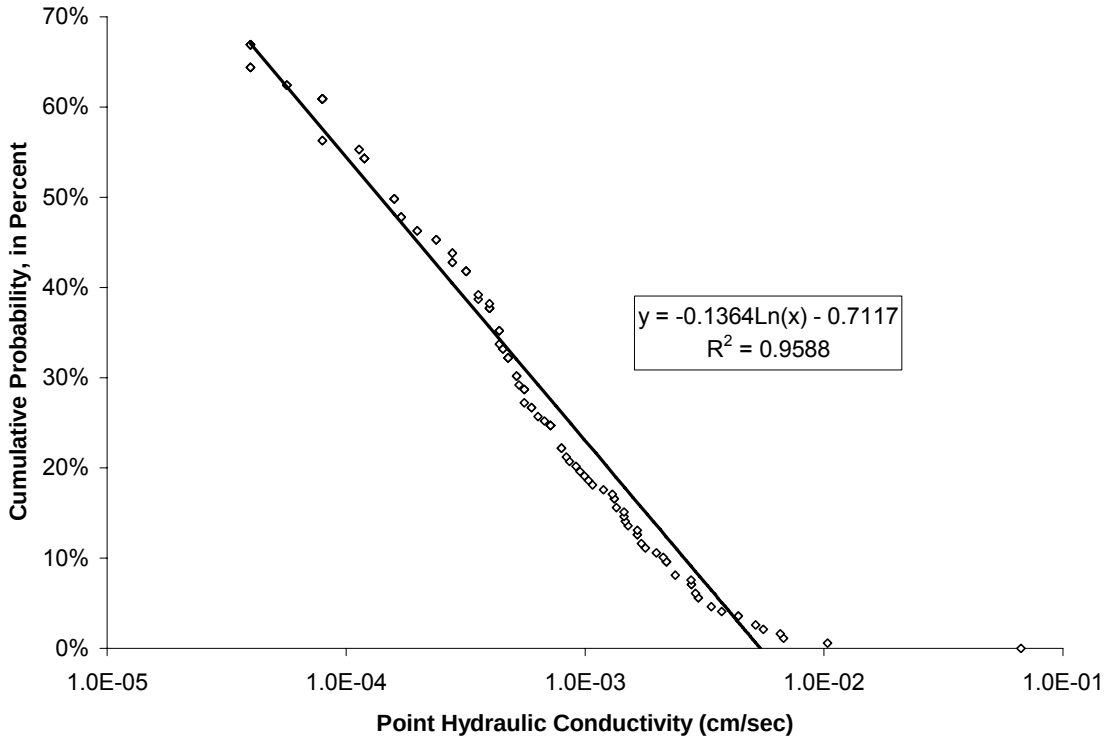

Figure 11: Frequency distribution of all point hydraulic conductivities.

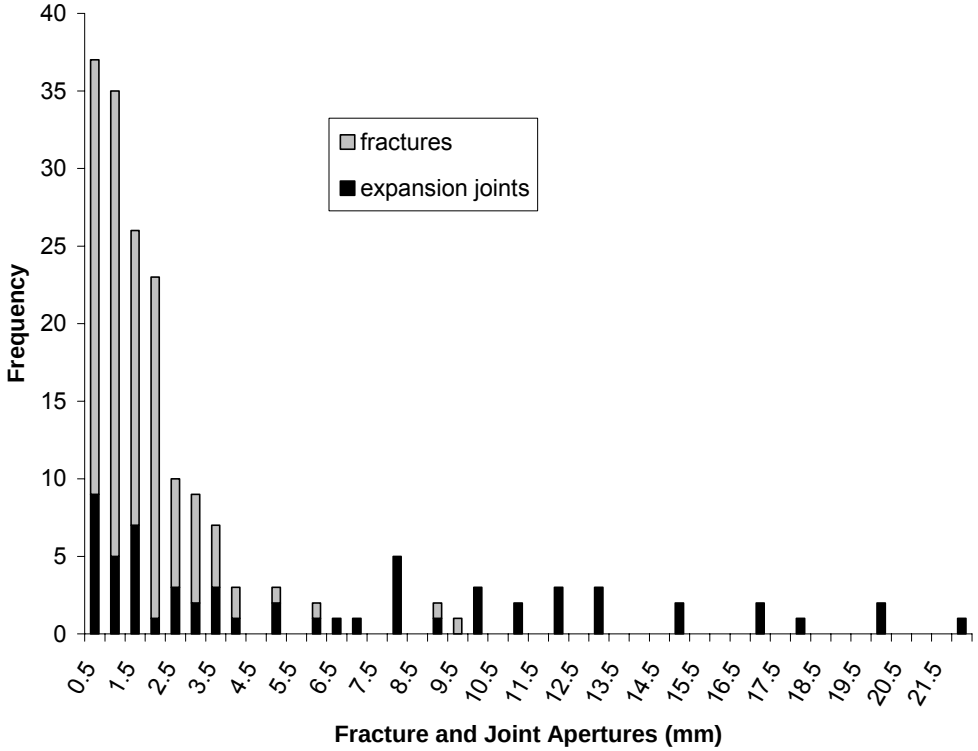

Figure 12: Histogram of all fracture and joint apertures. Apertures less than 0.5 mm are included in the first column.

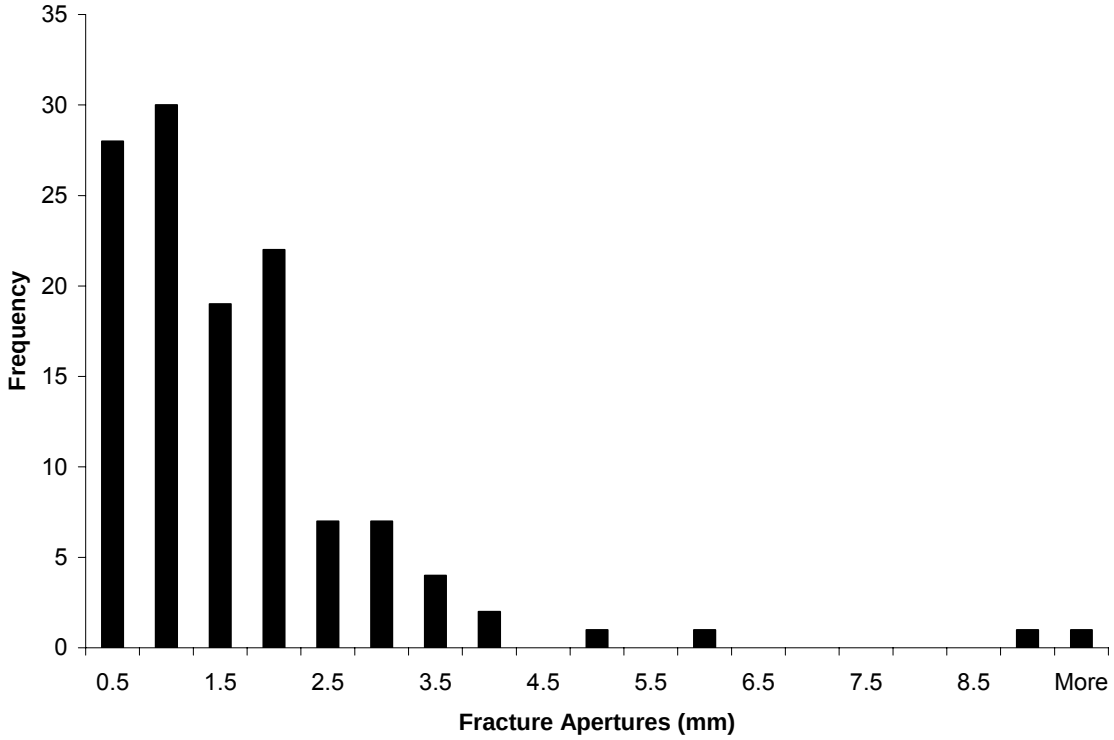

Figure 13: Histogram of fracture apertures only.

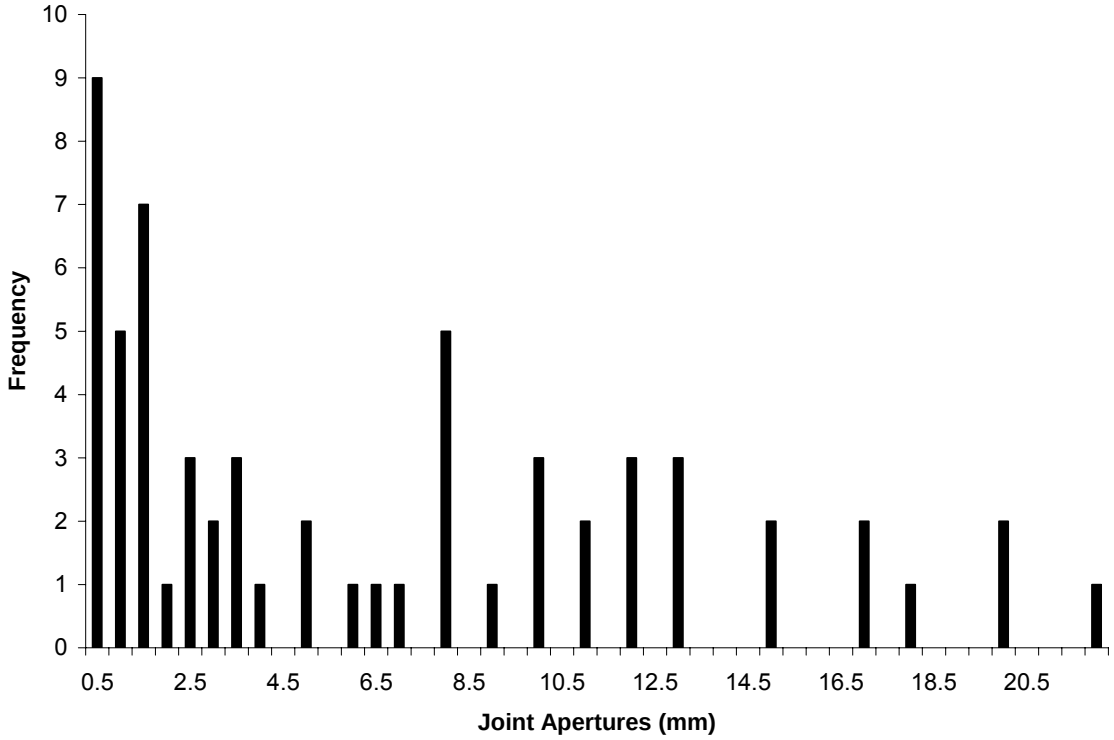

Figure 14: Histogram of expansion joint apertures only. Note bimodal distribution resulting from open (> 2.0 mm) versus closed joints (< 2.0 mm).

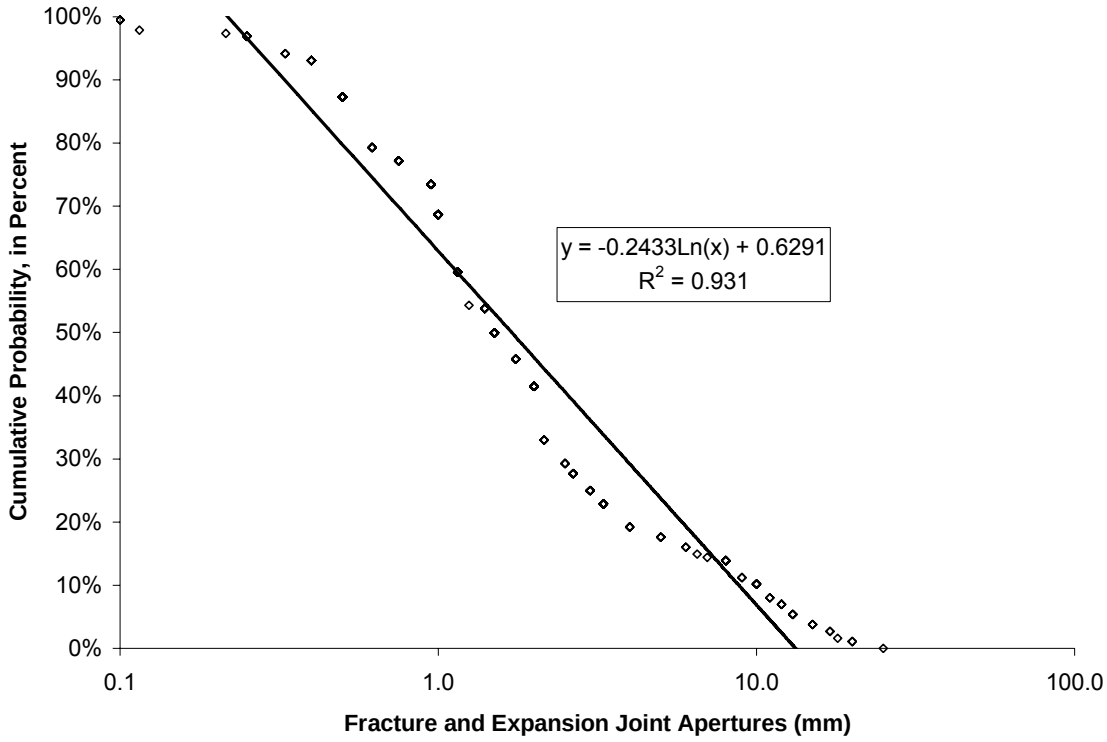

Figure 15: Frequency distribution of combined fracture and joint apertures.

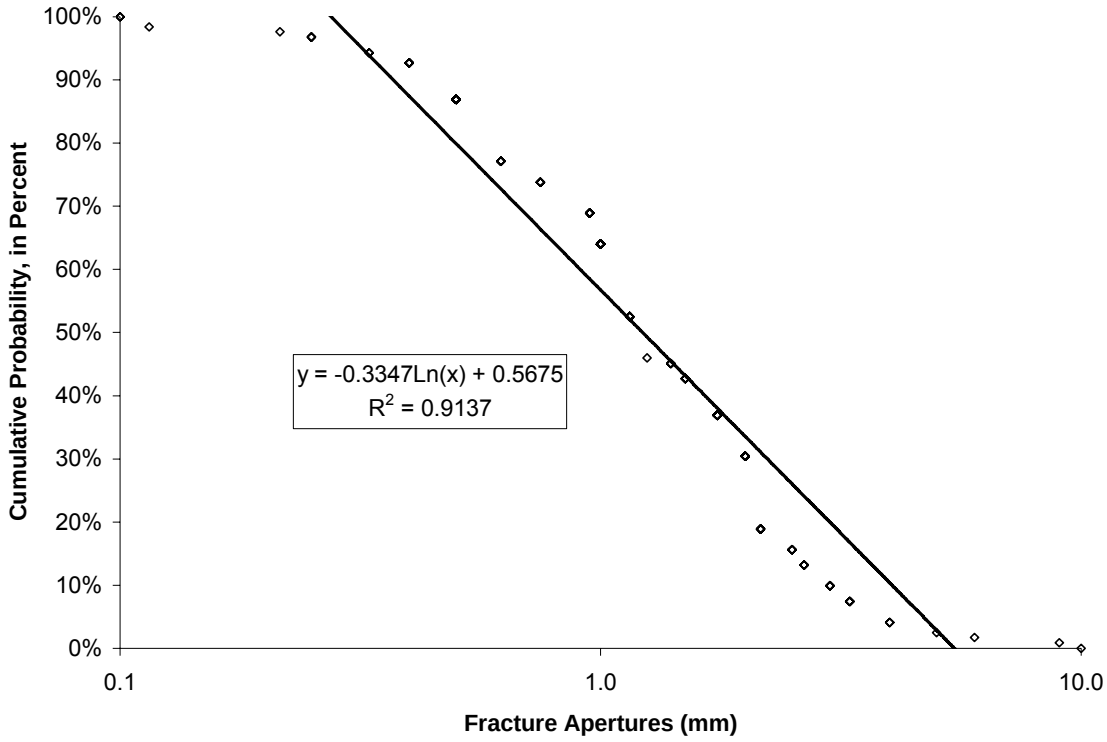

Figure 16: Frequency distribution of fracture apertures.

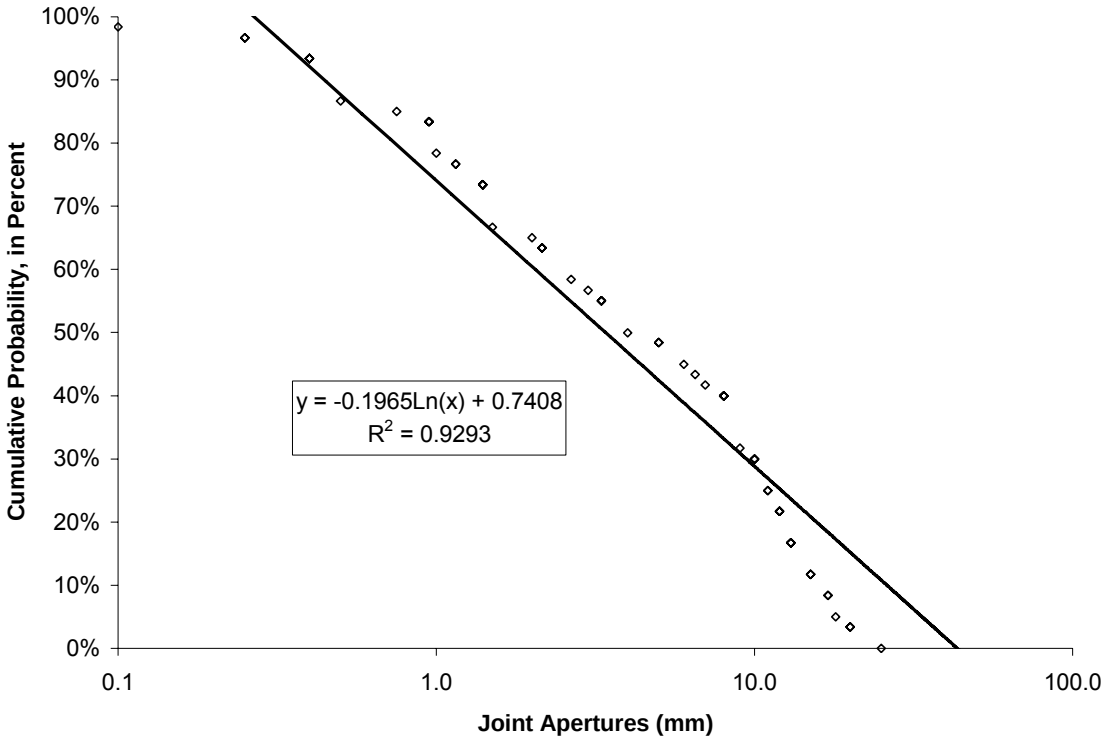

Figure 17: Frequency distribution of joint apertures.

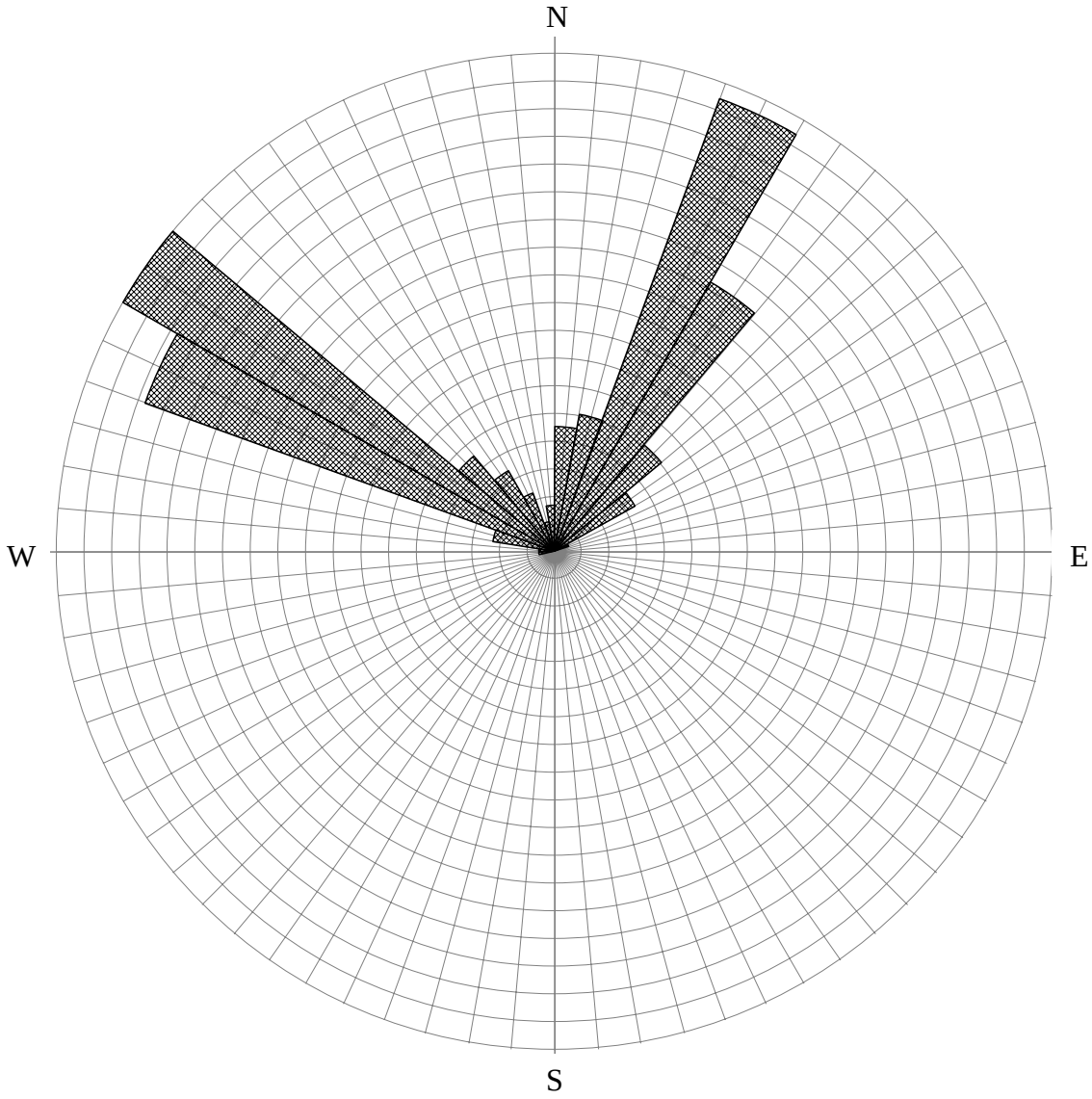

Figure 18: Rose diagram of all fracture and joint trends. The plotted trends are bi-directional (radius is 32).

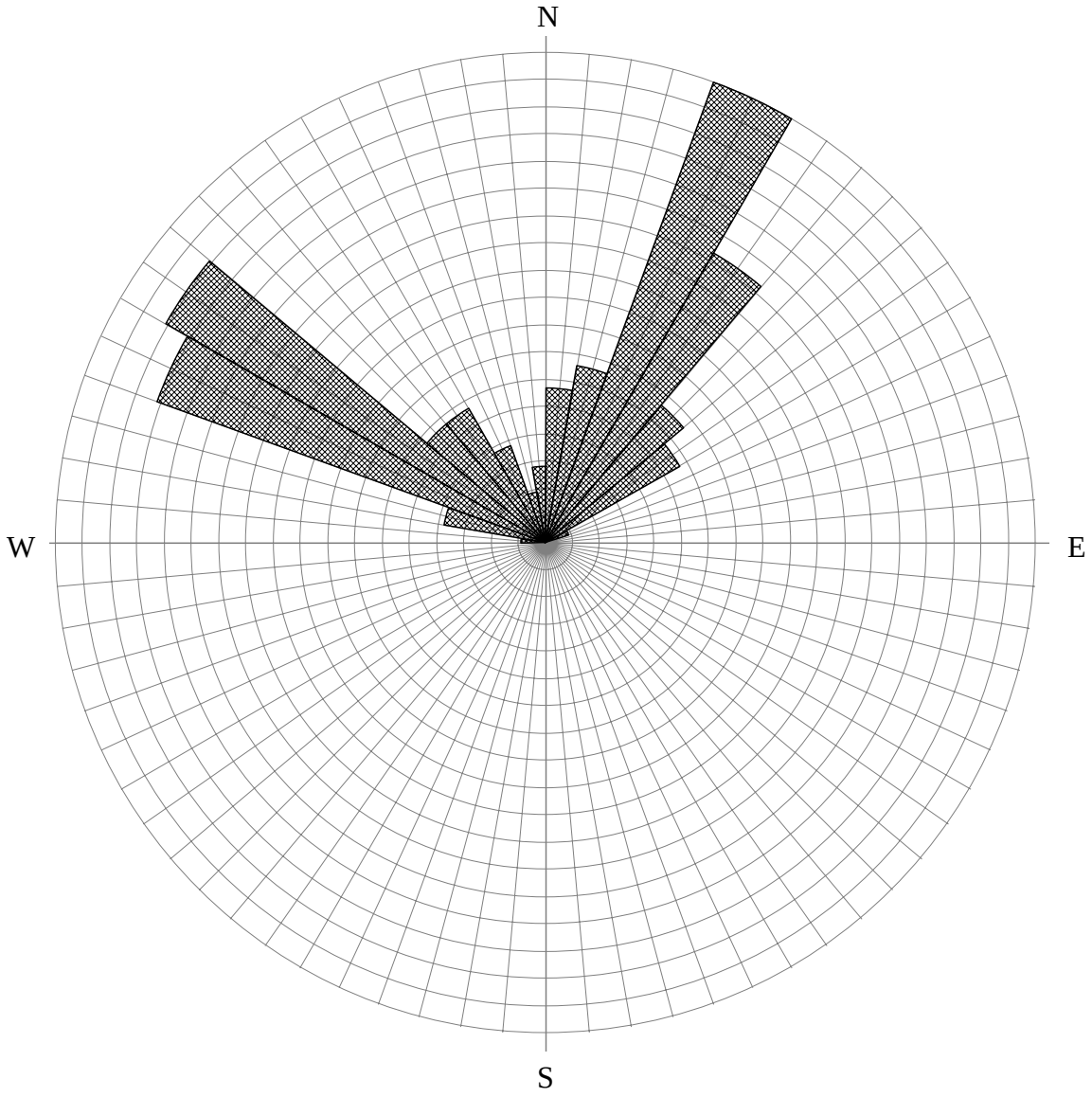

Figure 19: Rose diagram of fracture trends. The plotted trends are bi-directional (radius is 19).

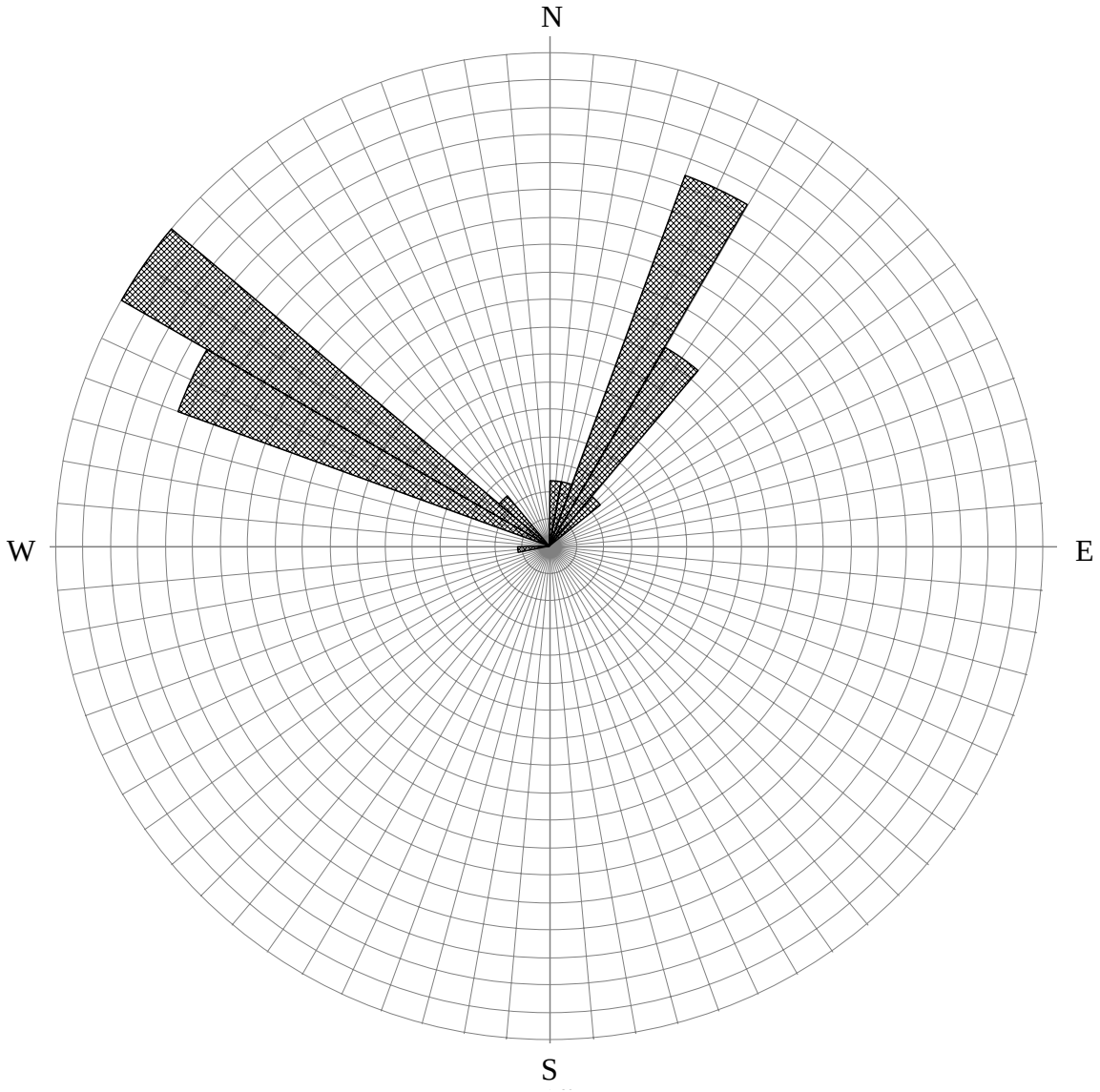

Figure 20: Rose diagram of joint trends. The plotted trends are bi-directional (radius is 15).

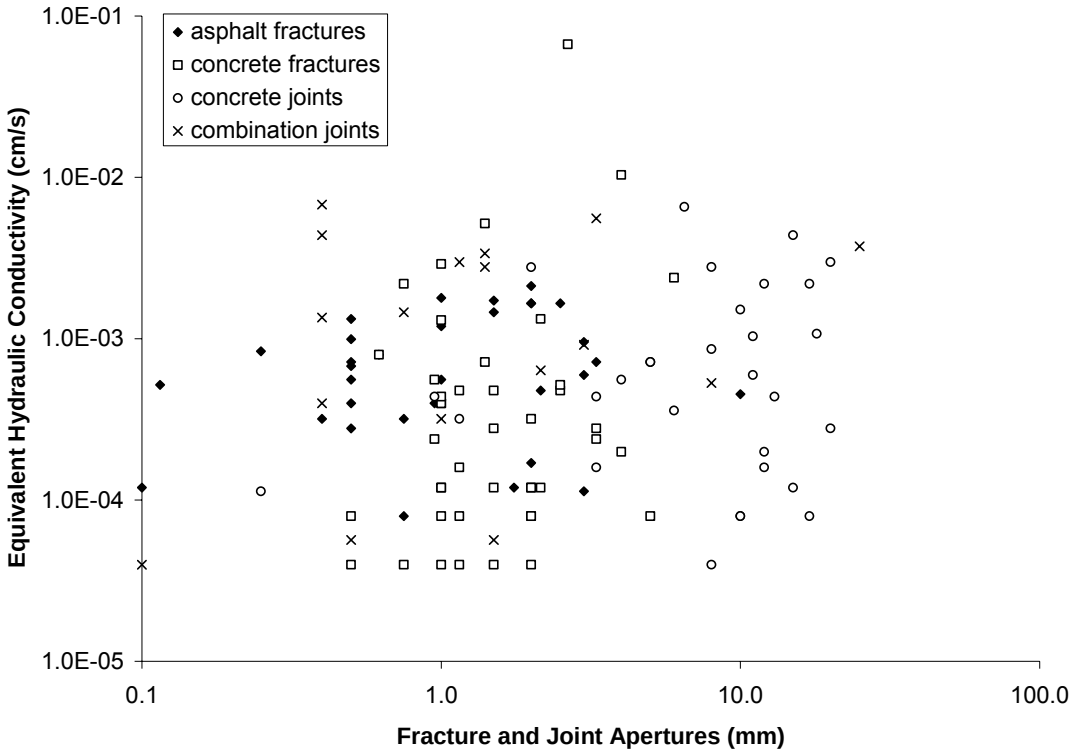

Figure 21: Equivalent hydraulic conductivities are plotted against apertures for joints and fractures in all pavement types and demonstrate that there is no correlation.

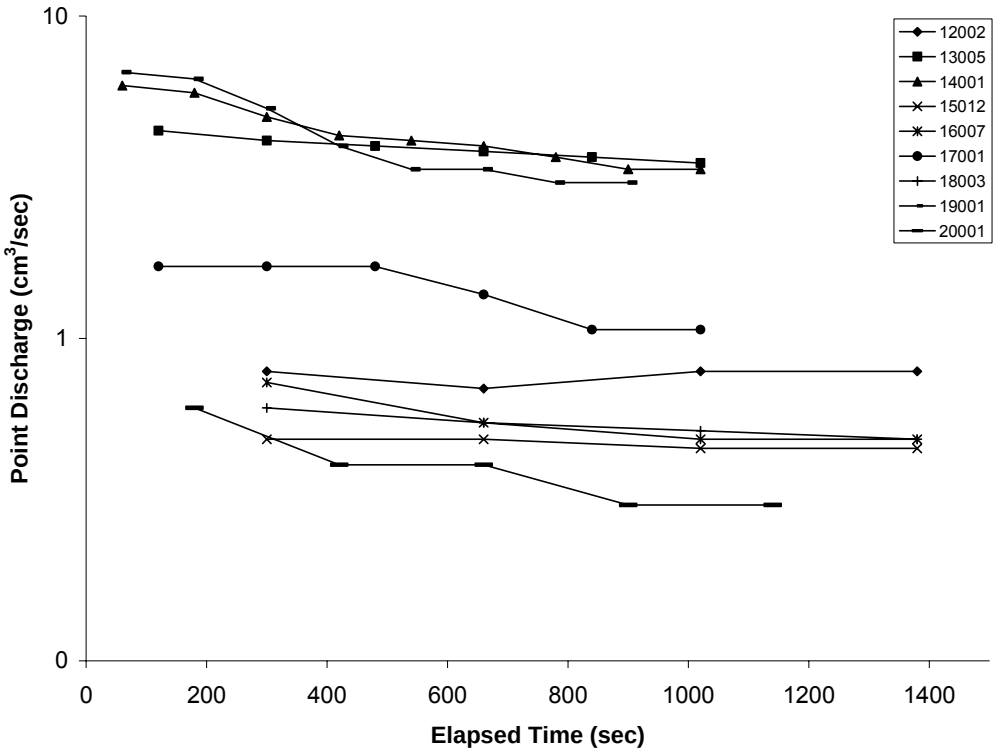

Figure 22: Time/discharge relation for select point on scanlines 12 through 20.

Table 3: Summary of scanline characteristics.

Hydrogeological Summary of Scanlines

16 scanlines - 30 meters per scanline
480 meters - cumulative scanline length

7 concrete curb gutters

Scanline	K_{eq} (cm/s)
19000	$4.1 \cdot 10^{-4}$
6000	$2.9 \cdot 10^{-5}$
17000	$2.5 \cdot 10^{-5}$
18000	$2.2 \cdot 10^{-5}$
16000	$1.6 \cdot 10^{-5}$
10000	$1.5 \cdot 10^{-5}$
20000	$3.2 \cdot 10^{-6}$

3 asphalt roads

Scanline	K_{eq} (cm/s)
8000	$2.9 \cdot 10^{-5}$
15000	$2.5 \cdot 10^{-5}$
12000	$1.2 \cdot 10^{-5}$

2.5 asphalt parking lots

Scanline	K_{eq} (cm/s
7000	$7.1 \cdot 10^{-5}$
14000	$3.7 \cdot 10^{-5}$

2.5 concrete parking lots

Scanline	K_{eq} (cm/s)
13000	$1.1 \cdot 10^{-4}$
9000	$8.5 \cdot 10^{-5}$
1000	$4.9 \cdot 10^{-5}$ *

1 concrete road

Scanline	K_{eq} (cm/s)
11000	$2.6 \cdot 10^{-6}$

* This value is the total equivalent hydraulic conductivity (K_{eq}) for scanline 1 which was half concrete and half asphalt

Table 4: Summary of sample point characteristics.

Fracture and Joint Hydraulic Summary

200 sample points - fractures and joints
134 with measurable K_{eq} ranging from $6.68 \cdot 10^{-2}$ cm/s to $3.98 \cdot 10^{-5}$ cm/s
66 had no measurable infiltration
all apertures ranged from 0.05 mm to 25.0 mm

Asphalt pavements

59 sample points
21 had no measurable infiltration

	K_{eq} Range (cm/s)		Aperture Range (mm)	
	High	**Low**	**Low**	**High**
49 fractures -	$2.12 \cdot 10^{-3}$	$7.95 \cdot 10^{-5}$	0.10	10.00
2 joints -	$2.39 \cdot 10^{-4}$	$7.95 \cdot 10^{-5}$	0.05	1.40
7 multi-fractures -	$4.53 \cdot 10^{-4}$	$5.66 \cdot 10^{-5}$		
1 intact -	0			

Concrete Pavements

121 sample points
44 had no measurable infiltration

	K_{eq} Range (cm/s)		Aperture Range (mm)	
	High	**Low**	**Low**	**High**
74 fractures -	$6.68 \cdot 10^{-2}$	$3.98 \cdot 10^{-5}$	0.25	9.00
41 joints -	$6.56 \cdot 10^{-3}$	$7.95 \cdot 10^{-5}$	0.25	20.00
4 multi-fractures -	$1.47 \cdot 10^{-3}$	$3.98 \cdot 10^{-5}$		
2 intact -	0			

Combination Pavements

20 sample points
1 had no measurable infiltration

	K_{eq} Range (cm/s)		Aperture Range (mm)	
	High	**Low**	**Low**	**High**
20 joints -	$6.76 \cdot 10^{-3}$	$3.98 \cdot 10^{-5}$	0.10	25.00

CHAPTER 4: INTERPRETATION AND DISCUSSION

DIRECT RECHARGE TRANSITIONS TO LOCALIZED RECHARGE

It can be reasonably stated that due to their low-permeability (effectively "impermeable") matrix, pavements decrease direct recharge. However, the decrease in direct recharge does not necessarily lead to an overall decrease in total recharge. Fractures and joints in the pavement were observed in this study to provide potential preferential flow paths for precipitation. Table 5 demonstrates that the equivalent hydraulic conductivity due to fractures and joints calculated for the overall paved surface in this study area, $5.9 \cdot 10^{-5}$ cm/s, should not be considered impervious; rather it is equivalent to very fine-grained sands, silts, or loams. These soil types are common in the alluvial deposits that dominate the surface geology in the Waller Creek Watershed.

While direct recharge decreases with urbanization, localized recharge increases dramatically. Fractures and expansion joints concentrate infiltration decreasing the time and volume of water necessary for saturation which leads to increased recharge potential. Previous studies indicate that localized recharge, particularly in arid or semi-arid regions, is the dominant and sometimes only source of recharge (Lerner, 1997a; DeVries and Simmers, 2002). Thus, it is likely that the increase in localized recharge can lead to an overall increase in total recharge.

CALCULATION OF POTENTIAL RECHARGE

Potential recharge is the portion of precipitation that infiltrates the surface and is available to recharge groundwater, provided it isn't held in the soil as soil moisture, captured by a shallow subsurface flow path as interflow, or intercepted in the root zone by vegetation. This study assumes saturated flow conditions through preferential flow

paths dominate flow, that interflow losses are negligible, and that the elimination of vegetation by paving the surface reduces or eliminates evapotranspiration. Once precipitation has infiltrated through the paved surface, it is potential recharge.

Precipitation Data

One way to calculate potential recharge is to multiply the infiltration flux by the amount of time that the surface can reasonably be expected to be saturated to the point of generating infiltration. The flux is determined in this study to be $5.9 \cdot 10^{-5}$ cm/s, which is equivalent to 2.1 mm/h. The wetted surface time depends on the number of precipitation events, the duration of those events, and their intensity. These parameters are available in the USGS Professional Paper 1725, Statistical Characteristics of Storm Interevent Time, Depth, and Duration for Eastern New Mexico, Oklahoma, and Texas (Asquith *et al.*, 2006).

A rainstorm is a period of non-zero rainfall followed by a period of zero rainfall. The *interoccurence interval* is the time period between two successive rainfall events (Asquith and Roussel, 2003). In any given storm there are likely to be brief periods of zero rainfall that do not constitute the end of one storm and the beginning of another. To distinguish between storm events, a minimum interoccurence interval should be stipulated. Because urban pavements are designed to have low depression storage, they quickly become saturated and begin to generate surface flow in response to even the smallest storms. In order to capture the effects of these small storms, the minimum interoccurence interval of 6 hours was used to select average storm characteristics for Travis County, Texas. These characteristics include a mean interevent time of 5.2 days, a mean storm duration of 5.77 hours, and a mean storm depth of 11.65 mm.

The general validity of these values can be determined by comparing them to the mean annual precipitation in Austin of 809 mm/year (Bomar, 1995). By dividing 365

days per year by the interevent time of 5.2 days, it is calculated that there are 70 storms per year in Travis County; multiplying by the mean storm depth of 11.65 mm, the resulting yearly rainfall is 815 mm which approximates closely the yearly rainfall observed by Bomar.

Before using these average data to calculate a potential recharge for pavements, it is necessary to address periods of zero rainfall within storms. Direct observation of storms during 6 years of residence in Austin allows one to conclude that it seldom, if ever, rains for 5.77 hours straight. Plots of the Natural Resources Conservation Service Type II and Type III hyetographs, which are appropriate for use in Texas, are shown on Figure 23. These hyetographs plot the percentage of storm depth versus the percentage of storm duration and indicate that the majority of the storm depth is produced in the middle 20 percent of the storm. Thus for the calculation of potential recharge the storm duration is adjusted to 20 percent of the total storm duration.

Potential Recharge

Using the adjusted rainfall data, the potential recharge through pavements from precipitation in Austin,Texas was determined by the calculation below to be 170 mm/y, which is 21 percent of annual precipitation. This estimate agrees with the infiltration estimates previously reported in Table 2.

$$70(events/year)\cdot 5.77(hours)\cdot 2.1(mm/h)\cdot 0.20(adjustment)=170(mm/year)$$

$$170mm/809mm = 21\%\ \ of\ annual\ precipitation$$

EVAPOTRANSPIRATION

Evapotranspiration consists of the combined effect of direct evaporation and *transpiration*, the uptake of water by plants. This study assumes that evapotranspiration is limited by these factors: high humidity, typically 100 percent during rain storms; the fact that once the water has infiltrated through the pavement it is effectively shielded from

evaporation; and that transpiration is all but eliminated by the removal of vegetation (DeVries and Simmers, 2002; van de Ven, 1990). The latter is certainly not the case for non-paved areas. It is commonly observed that recharge is much greater in non-vegetated areas than in vegetated ones. Gee *et al*. (1994) found that water storage increased over time from zero to as much as 50 percent of precipitation when plants were removed from the surface of their arid study sites and noted that vegetation appeared to control the water balance. It is reasonable to assume that the water balance is similarly affected by urbanization.

URBAN KARST

The term *urban karst* refers to the urban underground, which contains an intricate and rapidly changing system of trenches, tunnels, and other buried structures that alter the pre-urban porosity and permeability structure in a manner similar to the shaping of natural karst systems (Sharp *et al*., 2001). The permeability of natural karst aquifers is controlled by fractures and conduits which modify the host rock and provide for enhanced hydraulic conductivities (Halihan *et al.*, 1999) on the order of hundreds of meters per day.

Sharp *et al.* (2001) compare natural karst systems to urban systems by concluding that karstic systems have surface streams analogous to urban paved drainage ways; that internal drainage systems (dolines) are similar to storm drainage systems; and that permeability dominated by caves, fractures and conduits is very similar to permeability dominated by utility trenches, tunnels, and other conduits. In light of the permeability of pavements due to fractures and joints, it is logical to extend the idea of urban karst all the way to the surface. These preferential pathways provide infiltration of localized potential recharge into the urban karst network, which in turn provides preferential pathways by which to recharge groundwater.

Utility Trench Permeability

Practically every street in Austin is underlain by utility trenches of some sort—water lines, sanitary sewer lines, storm water sewer lines, and gas lines are ubiquitous. Many streets are under lain by all four major types of utilities. The trenches in which these utility lines rest were the subject of a study by Krothe (2001). Krothe collected permeability data from trench fill inside of utility trenches and from relatively undisturbed soil adjacent to the trench. All of these data were collected in areas overlain by Colorado River Alluvium. The mean hydraulic conductivity for undisturbed areas outside of the utility trenches was calculated to be $1.07 \cdot 10^{-5}$ (cm/s), and the mean for the fill material inside of the trenches was calculated to be $4.46 \cdot 10^{-4}$ (cm/s). These data, plotted in Figure 24, typically show more than a 2-orders-of-magnitude difference in hydraulic conductivity for conjugate pairs of data at each sample location, and demonstrate the profound effect utility trenches can have on near-surface permeability.

The Urban Septic Field

Utility systems create a network of interconnected conduits that have permeabilities as much as 6 orders of magnitude higher than the surrounding material (Sharp *et al*., 2001). The overall effect of urbanization on recharge can be viewed in terms of a septic system leach field. In a septic leach field, a system of trenches are excavated in low permeability surface strata; septic lines are installed; and the trenches are backfilled with highly permeable gravel or coarse sand. Waste water is delivered to the trenches and stored until it slowly leaches into the low permeability matrix. In the urban environment, preferential flow paths along fractures and joints act as the septic line, delivering rain water into the subsurface. The infiltrated water then drains into utility trenches, which approximate septic infiltration trenches.

Once rain water has entered the urban subsurface, it remains largely protected from evapotranspiration until it either passes directly into a higher permeability horizontal layer intersected by the trench; or travels laterally along the trench until intersecting a natural fracture or some other type of preferential pathway; or, after ponding, remains there under positive pressure, slowly infiltrating into the low permeability matrix material (Stephens, 1994).

PERMEABILITY SCALE EFFECTS

In karst aquifers, it has been observed that that permeability increases with scale and becomes dominated by conduit flow for large scales (Kiraly, 1975). Halihan *et al.* (1999) document a 4-orders-of-magnitude increase in permeability in carbonate rocks, from approximately 10^{-6} m/s at a laboratory scale to 10^{-2} m/s at a basin scale. Scale effects are not addressed in this study, but the pavements sampled were in relatively good repair and are not expected to have the highest concentration of permeable fractures and joints. Infiltration was found to be dominated by the most conductive fractures and joints, and permeability is likely to increase with scale as the most highly degraded pavements with the highest permeability preferential pathways are encountered.

EFFECTS OF LOCAL GEOLOGY

In the end the question of whether pavements are likely to enhance or retard recharge from precipitation is dominantly influenced by the surface geology of a given locale. In the unsaturated zone in the Waller Creek Watershed, material rarely is homogeneous. Alluvial deposits usually consist of layered sands, silts, and clays with wide variations in hydraulic conductivity. Areas with low surface permeability, whether due to low initial matrix permeability or to significant alteration during soil formation, are likely to have their permeability enhanced by the construction of paved surfaces and

utility networks. Areas with high surface permeabilities will likely experience a decrease in overall permeability.

In arid climates, where vegetation is efficient at removing moisture from the soil, development of low permeability caliche horizons is prevalent, and no provision for the runoff of storm water is made, the increased runoff either infiltrates surfaces through preferential flow paths or is lost to evapotranspiration (Lerner, 1997b). Scanlon (1990), as reported in Stephens (1994), found that a single fissure provided significant downward transport of fluids through calcareous paleosols which would otherwise be nearly impermeable. Under these circumstances urbanization is likely to increase recharge by increasing preferential flow paths. This is also the case in areas with surface geology that has a very low hydraulic conductivity, such as is exhibited by clay, unfractured rock, or some types of alluvium. Gee *et al*. (1994) found that when surface soils are silty loams, like alluvial overbank deposits, deep drainage is eliminated whether plants were present or not. But in areas where the surface geology has extremely high hydraulic conductivity, such as that found in unconsolidated, well-sorted sand or granite gruss, urbanization is likely to retard recharge.

URBAN PERMEABILITY RATIO METHOD

The question of how to account for pavements in the water balance still remains. The results of this study lead the author to propose a ratio method. The effect of pavements can be approximated by taking the ratio of the urban surface hydraulic conductivity to that of the dominant geologic surface cover. If the resulting ratio is much larger than 1, then pavements are likely to increase recharge; if the ratio is approximately 1, then pavements likely have little or no effect on recharge; if the ratio is significantly less than 1, then recharge is likely to decrease.

Effect of Pavements in the Waller Creek Watershed

The Waller Creek Watershed is dominantly covered by Colorado River Alluvium, where soil development on fine-grained flood materials creates low permeability zones (Sharp *et al.*, 2001). The average of the saturated hydraulic conductivities measured in undisturbed areas outside of utility trenches in Colorado River Alluvium by Krothe (2001) was determined to be $1.07 \cdot 10^{-5}$ cm/s, and hydraulic conductivity for pavements in the study area was determined to be $5.9 \cdot 10^{-5}$ cm/s. The ratio of pavement hydraulic conductivities (5.9/1.07) is much greater than 1, indicating that urbanization in the study area has increased precipitation recharge. When this effect is combined with the decrease in evapotranspiration due to pavement construction and with the increase in subsurface permeability engendered by utility trenches, it is a virtual certainty that no decrease in precipitation recharge occurs.

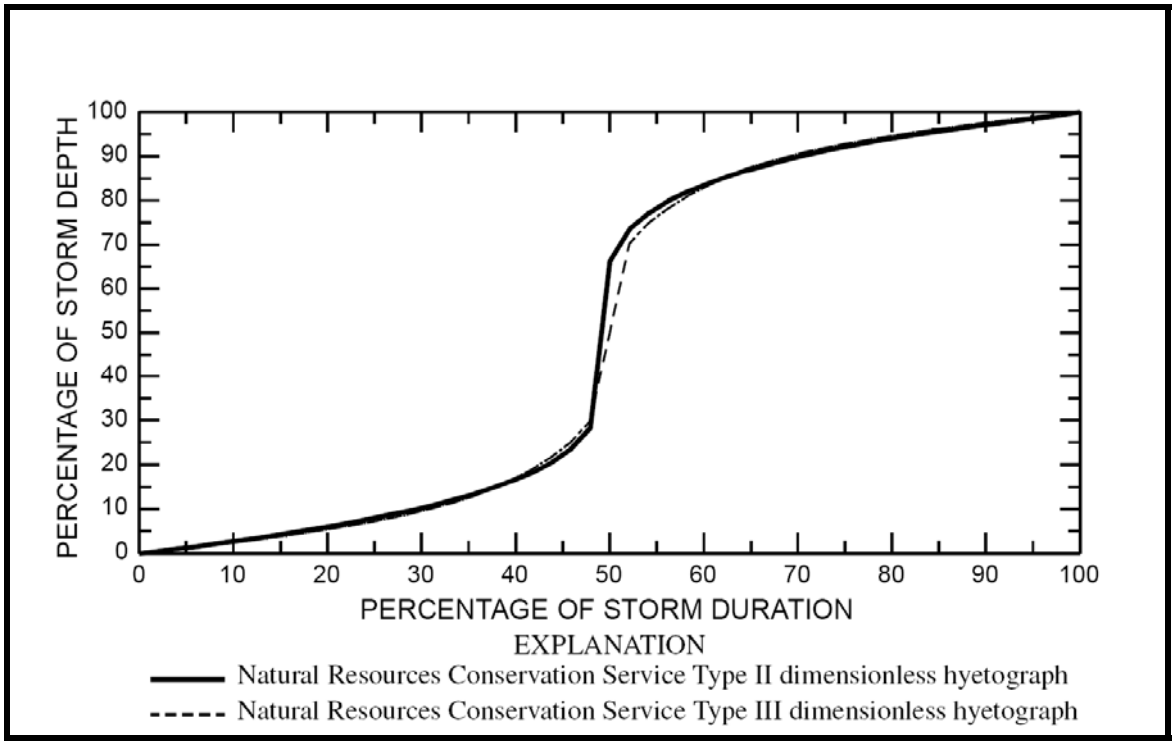

Figure 23: Hyetographs of storm depth versus storm duration applicable to storms in Texas (Reproduced from Asquith *et al.*, 2005).

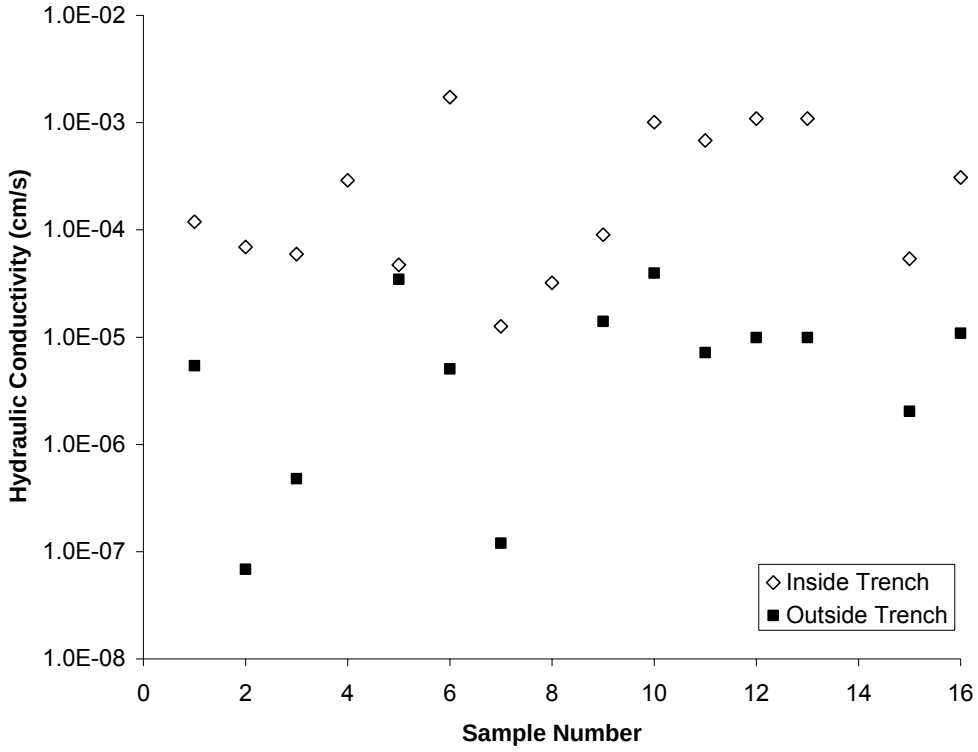

Figure 24: Guelph Permeameter hydraulic conductivity measurements for locations inside and outside of utility trenches excavated in Colorado River Alluvium (Modified from Krothe, 2001).

Table 5: Table of saturated hydraulic conductivities (Modified from Bear, 1972).

K (cm/s)	10^{2}	10^{1}	10^{0}	10^{-1}	10^{-2}	10^{-3}	10^{-4}	10^{-5}	10^{-6}	10^{-7}	10^{-8}	10^{-9}	10^{-10}
Relative Permeability	**Pervious**				**Semi-Pervious**					**Impervious**			
Aquifer	**Good**						**Poor**				**None**		
Soils	**Clean Gravel**			**Clean sand or sand and gravel**			**Very fine sand, silt, or loam**				**Unweathered Clay**		
Rocks	**Fractured rock formations**				**Resevoir rocks**			**Sandstone**		**Limestone and dolomite**			**Granite**
Urban Cover							**Roads and Parking lots**			**Roofs**			

CHAPTER 5: CONCLUSIONS AND FUTURE WORK

There is little doubt that urbanization alters groundwater recharge. The common wisdom has been that as an area urbanizes, impervious pavements—primarily roads and parking lots constructed of either concrete or asphalt—are responsible for a decrease in recharge. The results of this study indicate that this perception is flawed and that pavements are more likely to increase than decrease precipitation recharge.

There is no direct evidence of a decrease in precipitation recharge as a result of urbanization. In fact, except for one documented case, recharge in urban areas has been observed to be on the rise. The principal premise of the "precipitation recharge is decreasing" argument is that as an area urbanizes, storm runoff increases, and that as a result recharge necessarily must decrease. However, though storm peak discharges are higher in urbanized watersheds, runoff time is shorter, such that any increases in runoff volume are rather smaller than imagined. These differences in runoff volume are not directly attributable to decreases in recharge and are more reasonably explained by decreases in depression storage and evapotranspiration.

The reason that urbanization can’t be proven to decrease recharge is simply that urban pavements, which comprise the majority of “impervious cover,” are not impervious. As a result, except in areas with very high natural permeability, they don’t significantly inhibit infiltration. Even new pavements contain fractures and joints that are available as preferential pathways for infiltration of rain water. Thus, the decrease in direct recharge due to the effectively impermeable matrix of asphalt and concrete pavements is offset by an increase in localized recharge through fractures and joints. Overall recharge is likely to be unaffected or even to increase. Rainfall runoff studies conducted by sewer design engineers confirm the capacity of pavement to transmit

precipitation at rates as high as 27 mm/h, conserving as much as 40 percent of total rainfall.

The focus of this study was to determine the permeability of urban pavements. A double-ring infiltrometer was used to measure infiltration rates of 200 fractures and joints that were encountered along 16 scanlines on representative pavement types in the Waller Creek Watershed in Austin, Texas. Point-equivalent hydraulic conductivities were calculated directly from infiltration rates by assuming a unit gradient and were found to range from $6.68 \cdot 10^{-2}$ cm/s to $7.95 \cdot 10^{-5}$ cm/s for points with measurable infiltration (33 percent of the points exhibited no measurable infiltration). Scanline-equivalent hydraulic conductivities were determined by summing the point conductivities for each scanline and dividing by the area of the scanline, and were found to range from $4.1 \cdot 10^{-4}$ cm/s to $2.6 \cdot 10^{-6}$ cm/s. The total pavement hydraulic conductivity was determined by summing all of the point infiltration and dividing by the area represented by all of the scanlines, and was determined to be $5.9 \cdot 10^{-5}$ cm/s, which is the hydraulic conductivity of a fine-grained sand, silt, or loam. This value is 5 times higher than the average hydraulic conductivity found for relatively undisturbed areas with a surface geology dominated by alluvial deposits similar to those found in the study area.

Histogram and frequency plots of point fracture and joint characteristics show that point-hydraulic conductivities and point apertures are logarithmically distributed. However, a plot of apertures against hydraulic conductivity shows no correlation, leading to the conclusion that the fractures and joints are not rate limiting. The effects of both the fracture fills and the sub-grade provide the probable limits of infiltration and need to be further investigated. Additionally, rose diagrams of fracture and joint trends show them to form either sub-parallel or sub-perpendicular to pavement orientations, but because they

form sub-vertically to the surface, their orientations are not expected to have an effect on infiltration.

The hydraulic conductivity determined for pavements in this study, $5.9 \cdot 10^{-5}$ cm/s, is deemed to be appropriate for use in relatively well-maintained pavements overlying fine-grained alluvial deposits and may be used in conjunction with an estimate of the surface geology to determine how recharge is likely to be affected in similar locales. Further research is needed on more significantly distressed pavements and on pavements located over significantly different geologic conditions.

Urban pavements are permeable. The term “impervious cover” with respect to urban pavements is misleading both in definition and in the negative emotions it evokes, and its use ought to be discontinued. It would be far better to speak of pavements in terms of their significant permeability or hydraulic conductivity.

Other considerations in any assessment of the effects of urbanization on precipitation recharge are the extent of subsurface permeability modification—usually an increase—due to the installation of utilities, and the amount of decrease of evapotranspiration due to the removal of vegetation from construction sites. The combination of these factors with the demonstrated permeability of pavements can indeed lead to increases in precipitation recharge.

APPENDIX A

Fracture Permeability in Urban Pavements

Thomas J. Wiles
Urban Hydrogeology
Spring 2006

Introduction

Man is a geologic agent. Estimates show that the total amount of earth moved by humans in a given year is greater than all the sediment moved by all the rivers on the planet combined. Urban areas already comprise a significant portion—approximately 7%—of the land surface of the earth, and they continue to grow. With these facts in mind, it would seem reasonable that the effects of urbanization on the environment would be the subject of intense study and thus be well understood. Interestingly, though, our understanding of the effects of urbanization barely scratches the surface, and many long-held assumptions are turning out to be wrong.

Recent attempts to determine the effects of urbanization on groundwater levels have led to the observation that, contrary to what one would expect, groundwater levels tend to rise in urban areas (Sharp, 2006). Until recently it was assumed that urbanization increases impervious cover (buildings, roads, and parking lots), leading to decreased natural recharge and thus falling groundwater levels. A portion of this rise in groundwater levels may be attributed to anthropogenic recharge: leakage from sewer mains and water mains, watering lawns, and the like. However, the evidence also points to a problem with one of the basic assumptions about urbanization, namely, that roads and parking lots are impervious. A cursory glance at just about any urban pavement reveals that, far from being impervious, it contains both engineered expansion joints and fractures. Lerner, 2002, in light of these facts, estimated that roads and parking lots may be as much as 50% pervious.

A review of literature on the subject reveals that, while the permeability of unfractured concrete and asphalt pavemenst have been studied extensively, primarily by pavement engineers interested in ways both to increase recharge through the pavements and to protect paved surfaces, the study of permeability

in fractured pavements has been neglected. This paper is the first known attempt to quantify the flow through fractures and expansion joints and thus to truly quantify the permeability of urban pavements.

Methods

Three criteria were used to select the location for this experiment. The first was the necessity of a location with a sufficient amount and variety of fractures and expansion joints to sample. For the limited scope of this study, approximately twenty data points were determined to be sufficient. The second was the need to sample at least two pavement types, in this case asphalt and concrete. The last was proximity. Driving halfway across Austin was not feasible logistically. The parking lot located just outside the east basement door of the Jackson School of Geosciences building at the University of Texas at Austin was found to meet all of my criteria.

Experiment Design

The goal of the experiment was to determine the permeability of pavements due to fractures and expansion joints. In order to sample the pavement with minimal bias, I set up a 100-foot scan line, oriented approximately north-south, intersecting various types of expansion joints and fractures that began on concrete and terminated on asphalt. Infiltration tests were conducted at each point that a fracture or joint intersected the scan-line, as well as in adjacent unfractured areas of the different pavements. If, due to severely uneven surfaces, the fracture couldn't be sampled at the intersection then the fracture was sampled as close as possible to the scan-line. The cumulative infiltration rate or discharge could then be compared to the area of pavement represented by the scan-line to determine the equivalent fracture permeability. Also sampled were two additional areas which were not contained within the scan line, but

which represented the types of features that are often encountered on asphalt pavements.

Experimental Apparatus

In order to determine the infiltration rate of the various types of fractures and joints, I used a double-ring infiltrometer sealed to the pavement with plumber's putty. The double-ring configuration was necessary to prevent lateral flow in the fractures. Once the infiltrometer was sealed to the ground, the outer ring was filled to ensure that there was no leakage into the inner ring. This ensured that water would not leak through the seal into the outer ring, skewing the infiltration rate calculation. Once it was determined that there was no communication between the rings, both rings were filled to a depth of approximately six centimeters (an arbitrary water depth representing a level that was convenient to work with). After each infiltration test was conducted, measurements of the fracture length and average aperture through which flow was measured in the inner ring were recorded.

During the initial experiments, a Guelph Permeameter was used as a constant head device to maintain six centimeters of water in the inner ring of the infiltrometer. The level in the outer ring was kept at the same level as the inner ring by adding water manually. Measurements from the Guelph were recorded at even intervals during the experiments to determine the flux through the double ring. This configuration worked well at high flow rates. It was observed, however, that at very low flow rates the Guelph was unreliable. There were instances when the flow rate appeared to be negative when using the small diameter tube configurations. Thus, for each of the remaining sample locations a falling head test was conducted first. If the flow rate was determined to be sufficient, then the Guelph was employed to conduct a constant head test; if not, then only the initial falling head data were recorded. After the constant head test, a final falling head test was conducted for comparison to the first.

Data

In general, six types of fractures were sampled:

1. Open expansion joints with the original form lumber
2. Open expansion joints with sediment fill
3. Closed expansion joints
4. Simple fractures
5. Multi-fractures
6. Fracture swarms

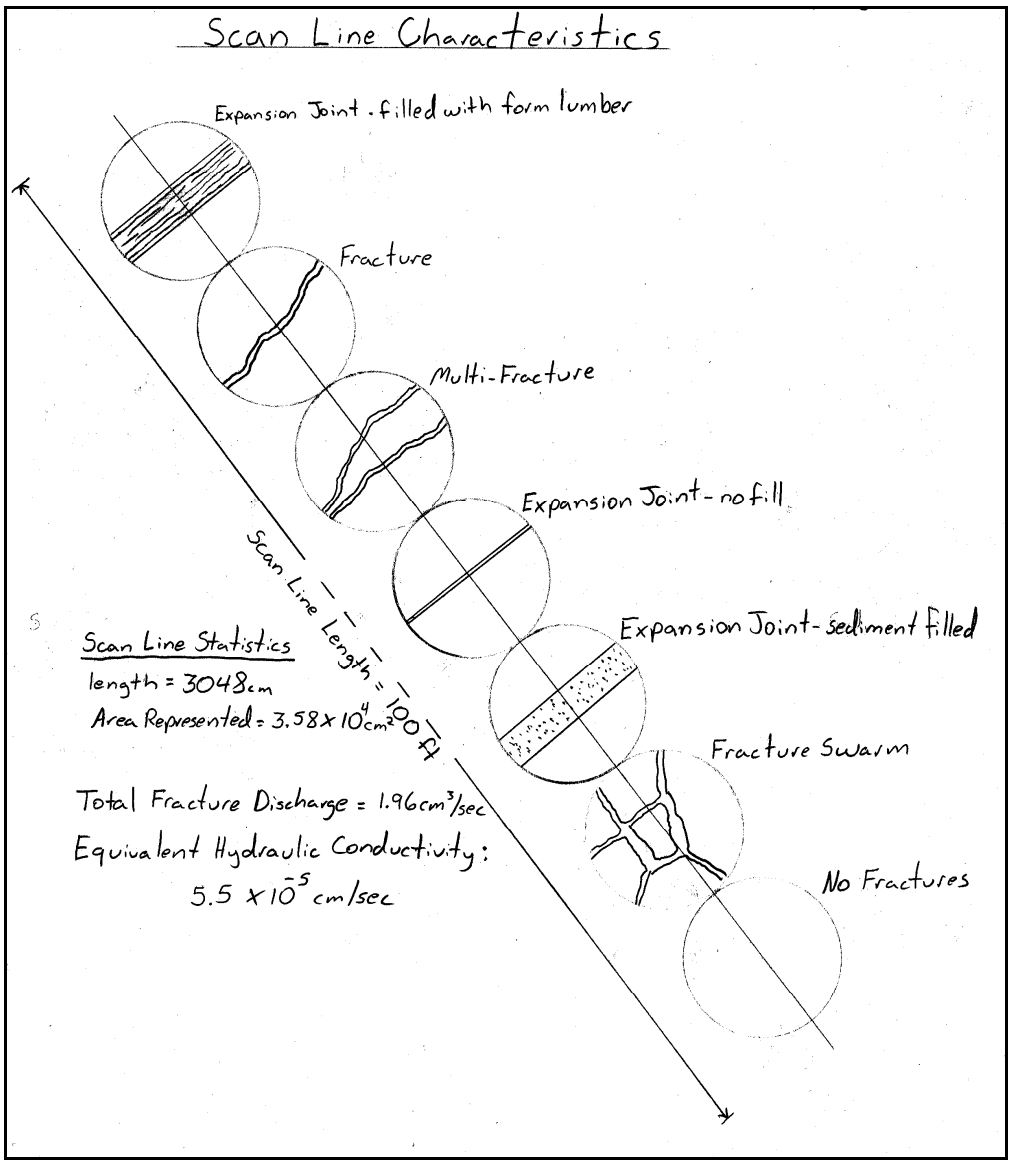

Figure 1 - A map view of fracture characteristics in the inner ring of the infiltrometer.

The data were collected at each sample location by measuring the height of the water column at the beginning of the test, and at succeeding increments of time, until the rate of change had clearly stabilized. Water height was measured using a millimeter-ruled ruler in the infiltrometer for the falling head tests, and using the internal millimeter graduations in the large ring of the Guelph Permeameter for the constant head tests. These changes in height of the water column were then

converted to volumes based on the change in volume per unit height of the different devices.

The data are presented on the following graphs as cumulative discharge in cubic centimeters per second versus elapsed time and have been separated on the basis of the type of pavement, concrete or asphalt, in which the fracture or joint was sampled. Sample 01-008 is an exception; it is included in the concrete analysis because it is a transition from concrete to asphalt and is typical of expansion joints in concrete.

Information about each location is provided on Table 1. Figure 2 presents the data from the constant head analysis which generally applied to concrete pavements with the exception of location 02-002. Figure 3 presents the data for the falling head analysis of fractures in concrete. These data are from the second falling head test only, because the method was not refined prior to the tests on the majority of these fractures. However, initial and final falling head tests were conducted for locations 01-006 and 01-008 and are presented on Figure 5. Figure 4 presents the falling head data for fractures in asphalt. Figure 5 presents the comparison of initial falling head test data and final falling head test data.

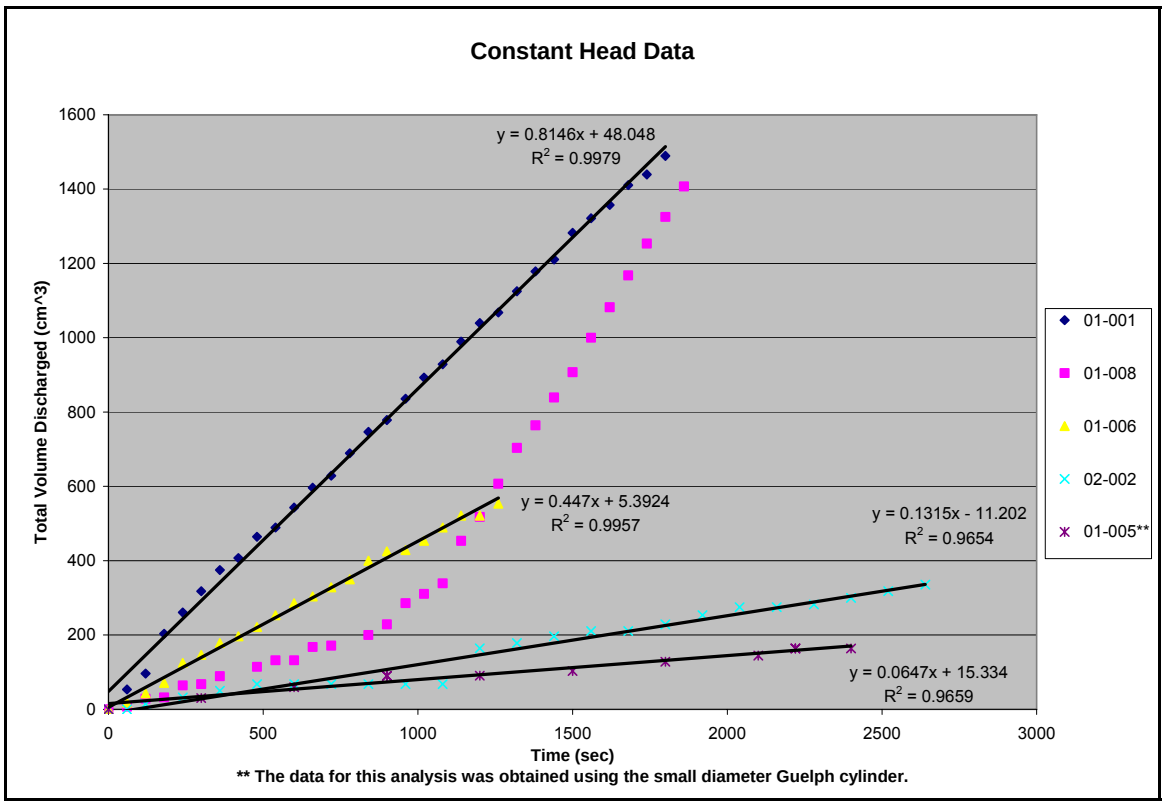

Figure 2 – This chart presents data from constant head analysis as total volume discharged per unit time. The slope of the best fit line gives the discharge in cm^3/sec.

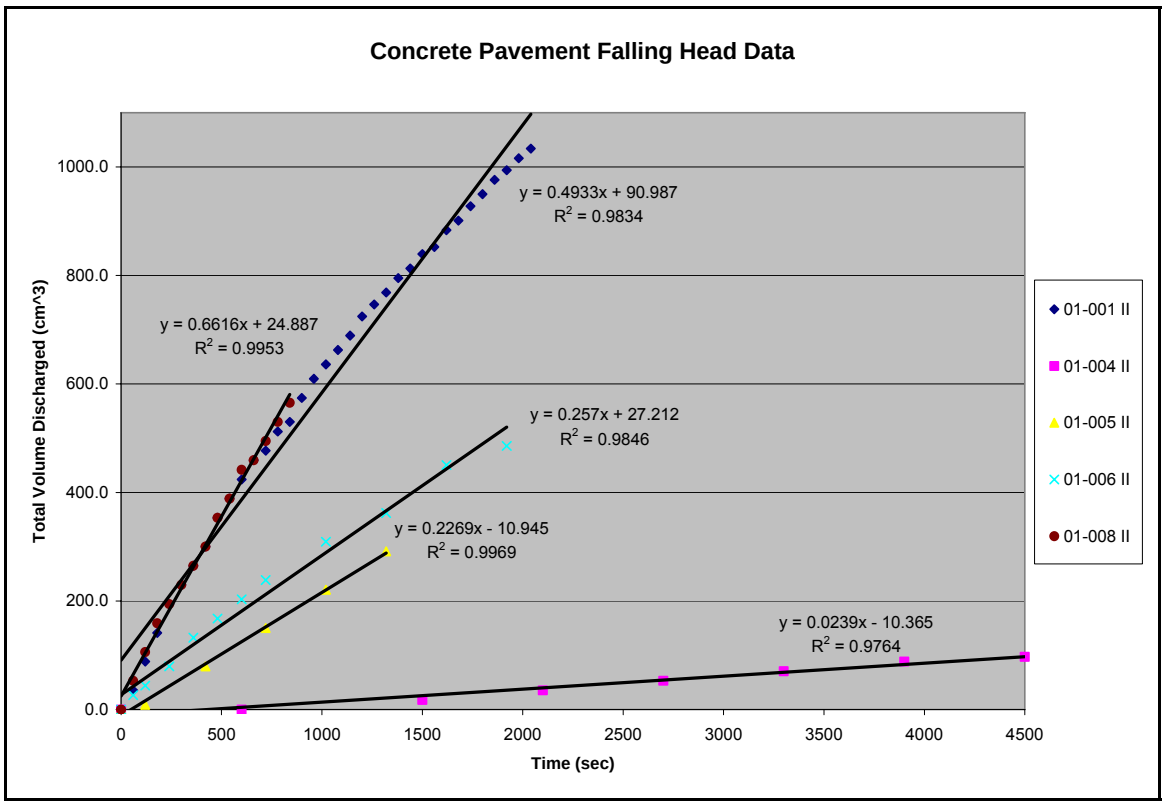

Figure 3 – This chart presents data from the final falling head tests on concrete pavements. Note that the discharge, as determined by the slope of the best fit line, are more conservative than constant head data.

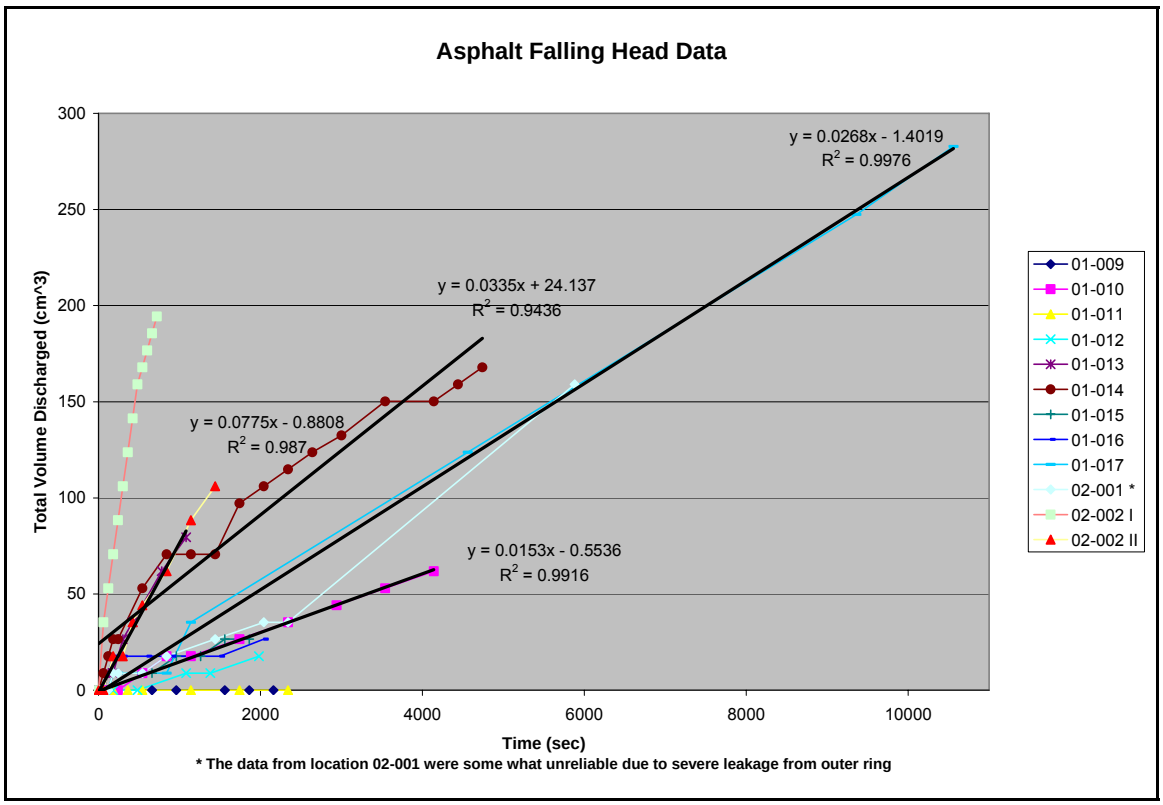

Figure 4 – This chart presents data collected from locations on the asphalt pavement. Again, fracture discharge can be determined by the slope of the best fit line.

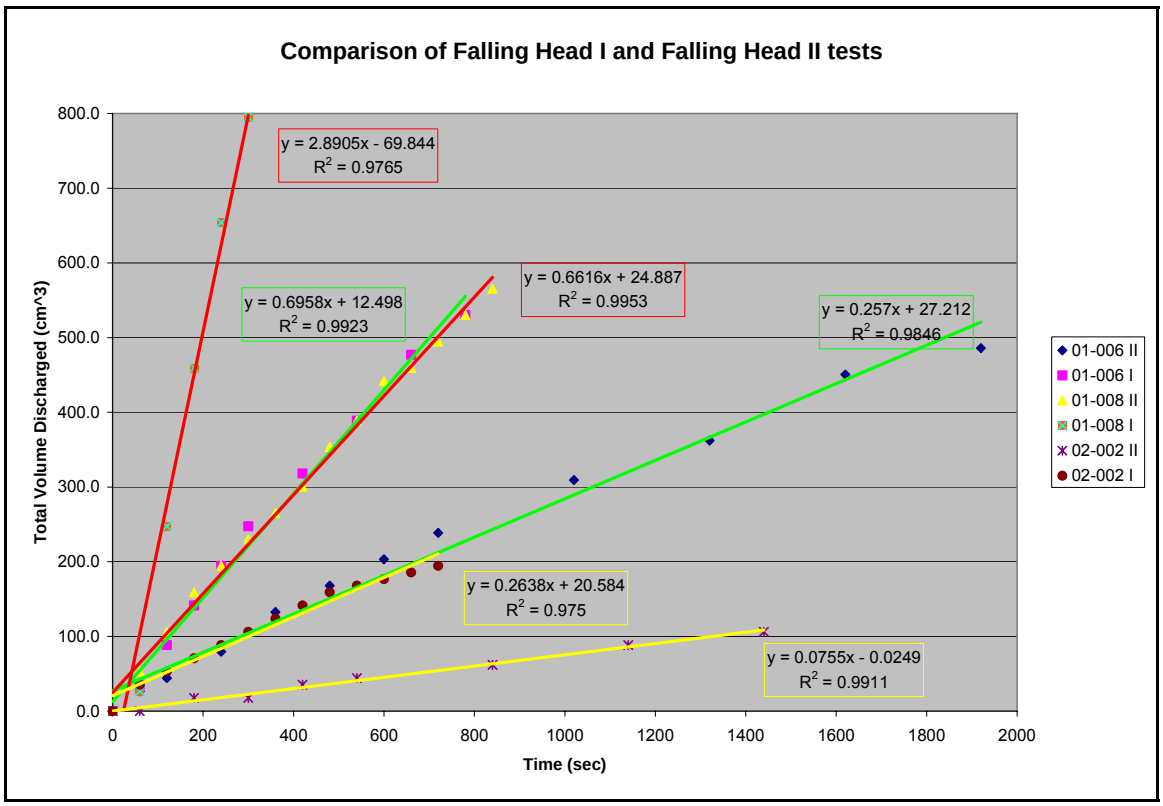

Figure 5 – This chart presents data from locations where both initial and final falling head data were collected. Note that initial discharge rates are approximately three times final discharge.

Table 1 - Location Data

Sample	Scan Line Location (ft from beginning)	Pavement Type	Category	Filler	Aperture (mm)	Length (cm)	Aperture (mm)	Length (cm)	Aperture (mm)	Length (cm)	Average Aperture (mm)	Discharge (cm^3/sec)	Fracture Trans. (cm^2/sec)
01-001	0.0	LG-CC/FG-CC	EJ	W	2.00	13.7	0.8	13.7			2.75	0.49	0.0358
01-002	NA	FG-CC	NF	NA	0.00						0.00	0.00	
01-003	NA	LG-CC	NF	NA	0.00						0.00	0.00	
01-004	1.4	LG-CC	EJ	NO	0.25	14.0					0.25	0.02	0.0014
01-005	7.6	LG-CC	F	S-FG	1.00	19.0					1.00	0.23	0.0121
01-006	9.4	LG-CC	MF	NO	0.50	13.0	0.5	13.0			0.50	0.26	0.0100
01-007	22.6	LG-CC	EJ	NO	0.25	13.5					0.25	0.00	0.0000
01-008	46.4	LG-CC/Asphalt	EJ	S FG/MG	25.00	13.5					25.00	0.66	0.0489
01-009	52.0	Asphalt	NF	NA	0.00						0.00	0.00	
01-010	55.4	Asphalt	F	NO	3.00	13.0					3.00	0.02	0.0015
01-011	62.0	Asphalt	F	NO	2.00	13.5					2.00	0.00	0.0000
01-012	66.0	Asphalt	MF	NO	2.00	13.5	1.0	6.0			1.69	0.01	0.0005
01-013	68.0	Asphalt	MF	NO	1.00	7.0	2.0	5.0	0.5	16.0	0.89	0.08	0.0029
01-014	70.6	Asphalt	FS	NO	1.00	20.0					1.00	0.03	0.0015
01-015	72.9	FG-CC/Asphalt	EJ/F	NO	0.50	14.0	0.5	7.0			0.50	0.01	0.0005
01-016	74.4	FG-CC/Asphalt	EJ	NO	1.50	14.0					1.50	0.01	0.0007
01-017	75.4	Asphalt	F	NO	2.00	14.0					2.00	0.03	0.0021
02-001	NA	Asphalt	FS	NO	0.50	30.0					0.50	0.03	0.0010
02-002	NA	Asphalt	F	S-FG	10.00	10.5					10.00	0.08	0.0076

Total Scan Line Discharge:	1.96

Symbols

EJ expansion joint
LG large grained
MG medium grained
FG fine grained
CC concrete
NF No visible fractures were present
W wood form lumber still intact
NA not applicable
NO not observed
S sediment
F fracture
MF multiple fractures
FS fracture swarm

Weighted average aperture was used to calculate fracture transmissiviy

Data Analysis

Figures 2, 3, and 4 demonstrate that closed expansion joints in concrete and fractures in asphalt have a much lower discharge than either open expansion joints or fractures in concrete. The problem, however, is that due to differences in aperture and fracture length in the tested locations, a direct comparison of discharge is not valid. In order to provide a means of direct comparison, I define the term: “fracture transmissivity”. Fracture transmissivity is simply the discharge divided by the fracture length. By comparing the weighted average aperture in each location to the fracture transmissivity (Figure 6), it becomes clear that asphalt fractures and closed expansion joints are approximately two orders of magnitude less transmissive than open expansion joints, and at least an order of magnitude less transmissive than fractures in concrete.

Fracture Transmissivity:

$$\frac{\text{Fracture Discharge (cm3/sec)}}{\text{Fracture Length (cm)}}$$

Weighted Average Aperture:

$$\frac{\text{Fracture length a x aperture a}}{\sum \text{fracture lengths}} + \frac{\text{fracture length b x aperture b}}{\sum \text{fracture lengths}}$$

Another interesting comparison is presented in Figure 5. The three locations in which data were collected for both initial falling head and final falling head are plotted to determine which discharge is more suitable for the ultimate calculation of equivalent fracture hydraulic conductivity (K_f). It becomes immediately clear that there is a two-to-three time decrease in discharge from the initial rate to the final rate. While it is not clear which rate would tend to dominate in a precipitation event, the more conservative rate was used to calculate the equivalent K_f.

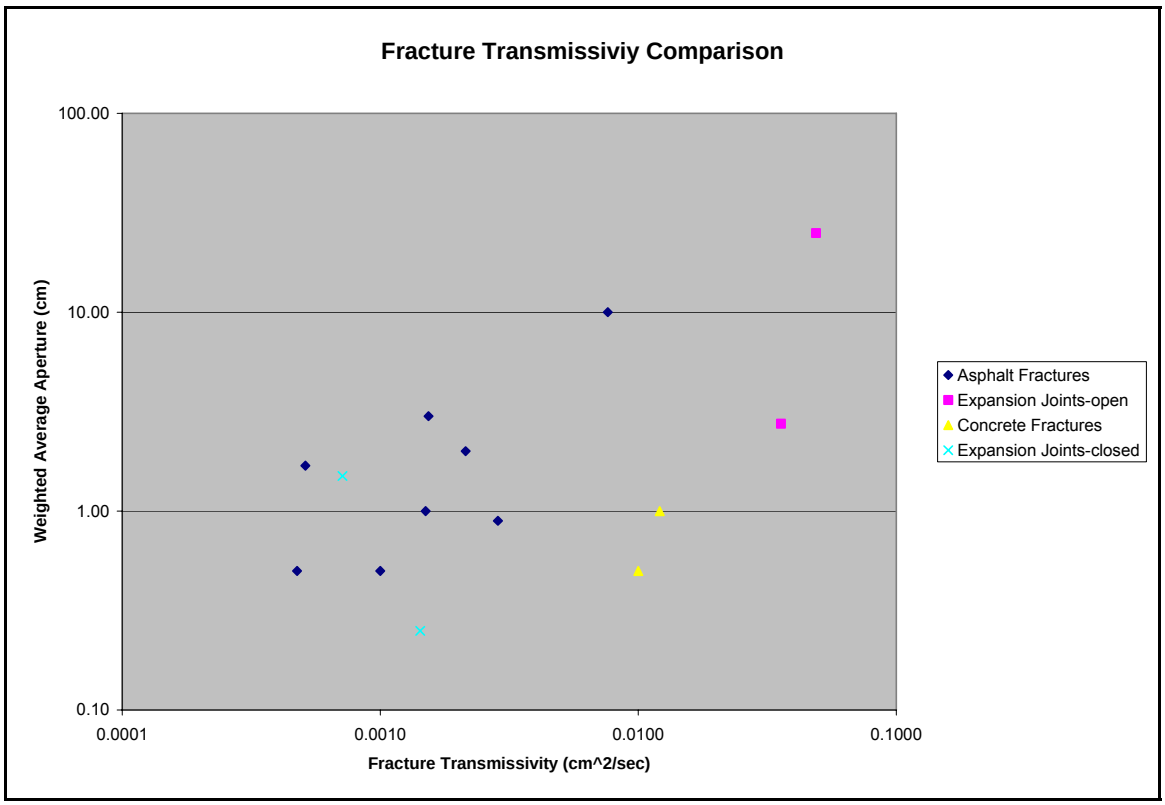

Figure 6 – This chart presents average aperture plotted versus fracture transmissivity data and is segregated by fracture class and pavement type. Because the expansion joints were found to have similar attributes regardless of pavement type they are classified as either open or closed.

In order to calculate an equivalent fracture hydraulic conductivity, I sum the areas of 15 cm circles that would fit edge to edge to determine the area represented by the scan line, and divide the sum of all the discharge rates by that area.

Equivalent Fracture Hydraulic Conductivity:

$$\frac{\text{Total Fracture Discharge } (cm^3/sec)}{\text{Scan Line Area } (cm^2)}$$

Excluding locations 02-001 and 02-002, which were not on the scan line, the total fracture discharge was determined to be 1.88 cm^3/sec. The total area represented by the 100-foot scan line was 3.58×10^4 cm^2. The resulting equivalent fracture hydraulic conductivity was calculated to be 5.25×10^{-5} cm/sec.

Discussion and Conclusions

It is clear that the scope of this study was extremely limited and that 19 sample points is inadequate to draw substantive conclusions. As they apply to the thin strip of pavement in the Jackson School of Geosciences at the University of Texas at Austin, I conclude the following:

1. Fractures in asphalt are less fracture transmissive than those in concrete.
2. Open expansion joints have the highest fracture transmissivities.
3. Closed expansion joints have the lowest transmissivities.
4. Initial infiltration rates for falling head tests are approximately three times higher than those observed after approximately an hour of infiltration.
5. The equivalent fracture hydraulic conductivity for the area of the scan line was 10^{-5} cm/s, which is roughly equivalent to very fine sand.

My purpose in this study was not to make specific predictions of urban pavements in general, but to investigate a hypothesis and develop methods for future analysis. In that, I believe I have succeeded. The data show that the parking lot is not impervious at all. In areas with low surface hydraulic conductivity, it may turn out that building roads and parking lots actually increases recharge. This study highlights the need for future research in this area.

References

Bear, Jacob, 1972, Dynamics of Fluids in Porous Media, American Elsevier Publishing Company, Inc.

Gulden, Lindsey, 2006, Representation of urban landscapes in climate and weather models, In class presentation: Urban Hydrogeology, The Jackson School of Geosciences, The University of Texas at Austin.

Lerner, D.N., 2002, Identifying and quantifying urban recharge: a review: Hydrogeology Journal, v. 10, p. 143-152.

Sharp, J.M., 2006, Oral Communication: Lectures in Urban Hydrogeology, The Jackson School of Geosciences, The University of Texas at Austin.

APPENDIX B

Bench Test Data - Falling Head Analysis 04-003

Sample	Date	Depth Range (cm)	Outer Ring Depth (cm)	Average Depth (cm)	Δ Time (s)	Aperture (mm)	Sub Grade
04-003	10/4/2006	8-7	7.5	7.5	4.53	0.25	pea gravel
04-003	10/4/2006	8-7	7.5	7.5	4.44	0.25	pea gravel
04-003	10/4/2006	8-7	7.5	7.5	4.47	0.25	pea gravel
04-003	10/4/2006	7-6	6.5	6.5	4.56	0.25	pea gravel
04-003	10/4/2006	7-6	6.5	6.5	4.91	0.25	pea gravel
04-003	10/4/2006	7-6	6.5	6.5	4.68	0.25	pea gravel
04-003	10/4/2006	6-5	5.5	5.5	4.91	0.25	pea gravel
04-003	10/4/2006	6-5	5.5	5.5	5.06	0.25	pea gravel
04-003	10/4/2006	6-5	5.5	5.5	5.16	0.25	pea gravel
04-003	10/4/2006	5-4	4.5	4.5	5.25	0.25	pea gravel
04-003	10/4/2006	5-4	4.5	4.5	5.38	0.25	pea gravel
04-003	10/4/2006	5-4	4.5	4.5	5.22	0.25	pea gravel
04-003	10/4/2006	4-3	3.5	3.5	5.97	0.25	pea gravel
04-003	10/4/2006	4-3	3.5	3.5	5.81	0.25	pea gravel
04-003	10/4/2006	4-3	3.5	3.5	5.72	0.25	pea gravel
04-003	10/4/2006	3-2	2.5	2.5	6.41	0.25	pea gravel
04-003	10/4/2006	3-2	2.5	2.5	6.56	0.25	pea gravel
04-003	10/4/2006	3-2	2.5	2.5	6.66	0.25	pea gravel
04-003	10/4/2006	2-1	1.5	1.5	6.87	0.25	pea gravel
04-003	10/4/2006	2-1	1.5	1.5	6.81	0.25	pea gravel
04-003	10/4/2006	2-1	1.5	1.5	6.72	0.25	pea gravel
04-003	10/4/2006	1-0	0.5	0.5	7.13	0.25	pea gravel
04-003	10/4/2006	1-0	0.5	0.5	6.97	0.25	pea gravel
04-003	10/4/2006	1-0	0.5	0.5	6.50	0.25	pea gravel

Bench Test Data - Falling Head Analysis 04-005

Sample	Date	Depth Range (cm)	Outer Ring Depth (cm)	Average Depth (cm)	Δ Time (s)	Aperture (mm)	Sub Grade
04-005	10/4/2006	8-7	8.0	7.5	16.31	0.1	pea gravel
04-005	10/4/2006	8-7	8.0	7.5	16.56	0.1	pea gravel
04-005	10/4/2006	8-7	8.0	7.5	16.94	0.1	pea gravel
04-005	10/4/2006	7-6	7.0	6.5	17.66	0.1	pea gravel
04-005	10/4/2006	7-6	7.0	6.5	18.40	0.1	pea gravel
04-005	10/4/2006	7-6	7.0	6.5	18.06	0.1	pea gravel
04-005	10/4/2006	6-5	6.0	5.5	19.25	0.1	pea gravel
04-005	10/4/2006	6-5	6.0	5.5	19.43	0.1	pea gravel
04-005	10/4/2006	6-5	6.0	5.5	19.29	0.1	pea gravel
04-005	10/4/2006	5-4	5.0	4.5	20.88	0.1	pea gravel
04-005	10/4/2006	5-4	5.0	4.5	20.59	0.1	pea gravel
04-005	10/4/2006	5-4	5.0	4.5	20.62	0.1	pea gravel
04-005	10/4/2006	4-3	4.0	3.5	22.66	0.1	pea gravel
04-005	10/4/2006	4-3	4.0	3.5	22.69	0.1	pea gravel
04-005	10/4/2006	4-3	4.0	3.5	22.75	0.1	pea gravel
04-005	10/4/2006	3-2	3.0	2.5	25.50	0.1	pea gravel
04-005	10/4/2006	3-2	3.0	2.5	25.03	0.1	pea gravel
04-005	10/4/2006	3-2	3.0	2.5	25.06	0.1	pea gravel
04-005	10/4/2006	2-1	2.0	1.5	29.50	0.1	pea gravel
04-005	10/4/2006	2-1	2.0	1.5	29.44	0.1	pea gravel
04-005	10/4/2006	2-1	2.0	1.5	29.59	0.1	pea gravel
04-005	10/4/2006	1-0	1.0	0.5	25.85	0.1	pea gravel
04-005	10/4/2006	1-0	1.0	0.5	25.75	0.1	pea gravel
04-005	10/4/2006	1-0	1.0	0.5	26.69	0.1	pea gravel

Bench Test Data - Falling Head Analysis 04-007

Sample	Date	Depth Range (cm)	Outer Ring Depth (cm)	Average Depth (cm)	Δ Time (s)	Aperture (mm)	Sub Grade
04-007	10/13/2006	8-7	8.0	7.5	8.37	0.075	coarse sand
04-007	10/13/2006	8-7	8.0	7.5	8.34	0.075	coarse sand
04-007	10/13/2006	8-7	8.0	7.5	8.18	0.075	coarse sand
04-007	10/13/2006	7-6	7.0	6.5	8.63	0.075	coarse sand
04-007	10/13/2006	7-6	7.0	6.5	8.72	0.075	coarse sand
04-007	10/13/2006	7-6	7.0	6.5	8.63	0.075	coarse sand
04-007	10/13/2006	6-5	6.0	5.5	9.56	0.075	coarse sand
04-007	10/13/2006	6-5	6.0	5.5	9.25	0.075	coarse sand
04-007	10/13/2006	6-5	6.0	5.5	9.31	0.075	coarse sand
04-007	10/13/2006	5-4	5.0	4.5	9.82	0.075	coarse sand
04-007	10/13/2006	5-4	5.0	4.5	9.78	0.075	coarse sand
04-007	10/13/2006	5-4	5.0	4.5	9.78	0.075	coarse sand
04-007	10/13/2006	4-3	4.0	3.5	10.72	0.075	coarse sand
04-007	10/13/2006	4-3	4.0	3.5	10.40	0.075	coarse sand
04-007	10/13/2006	4-3	4.0	3.5	10.53	0.075	coarse sand
04-007	10/13/2006	3-2	3.0	2.5	11.84	0.075	coarse sand
04-007	10/13/2006	3-2	3.0	2.5	11.50	0.075	coarse sand
04-007	10/13/2006	3-2	3.0	2.5	11.87	0.075	coarse sand
04-007	10/13/2006	2-1	2.0	1.5	13.59	0.075	coarse sand
04-007	10/13/2006	2-1	2.0	1.5	13.28	0.075	coarse sand
04-007	10/13/2006	2-1	2.0	1.5	13.62	0.075	coarse sand
04-007	10/13/2006	1-0	1.0	0.5	11.16	0.075	coarse sand
04-007	10/13/2006	1-0	1.0	0.5	11.41	0.075	coarse sand
04-007	10/13/2006	1-0	1.0	0.5	11.69	0.075	coarse sand

Bench Test Data - Constant Head 04-004, 04-006, 04-008

Sample	Date	Outer Ring Depth (cm)	Inner Ring Depth (cm)	Δ Time (s)	Volume Discharged (ml)	Aperture (mm)	Sub Grade
04-004	10/4/2006	1	1	30	720	0.25	pea gravel
04-004	10/4/2006	1	1	30	728	0.25	pea gravel
04-004	10/4/2006	1	1	30	725	0.25	pea gravel
04-004	10/4/2006	2	2	30	815	0.25	pea gravel
04-004	10/4/2006	2	2	30	815	0.25	pea gravel
04-004	10/4/2006	2	2	30	815	0.25	pea gravel
04-004	10/4/2006	4	4	30	972	0.25	pea gravel
04-004	10/4/2006	4	4	30	975	0.25	pea gravel
04-004	10/4/2006	8	8	30	1255	0.25	pea gravel
04-004	10/4/2006	8	8	30	1238	0.25	pea gravel
04-006	10/4/2006	1	1	60	262	0.1	pea gravel
04-006	10/4/2006	1	1	60	262	0.1	pea gravel
04-006	10/4/2006	2	2	60	368	0.1	pea gravel
04-006	10/4/2006	2	2	60	368	0.1	pea gravel
04-006	10/4/2006	4	4	60	468	0.1	pea gravel
04-006	10/4/2006	4	4	60	468	0.1	pea gravel
04-006	10/4/2006	8	8	30	325	0.1	pea gravel
04-006	10/4/2006	8	8	30	325	0.1	pea gravel
04-008	10/13/2006	1	1	60	710	0.075	coarse sand
04-008	10/13/2006	1	1	60	715	0.075	coarse sand
04-008	10/13/2006	2	2	30	385	0.075	coarse sand
04-008	10/13/2006	2	2	30	385	0.075	coarse sand
04-008	10/13/2006	4	4	30	508	0.075	coarse sand
04-008	10/13/2006	4	4	30	510	0.075	coarse sand
04-008	10/13/2006	8	8	30	710	0.075	coarse sand
04-008	10/13/2006	8	8	30	710	0.075	coarse sand

APPENDIX C

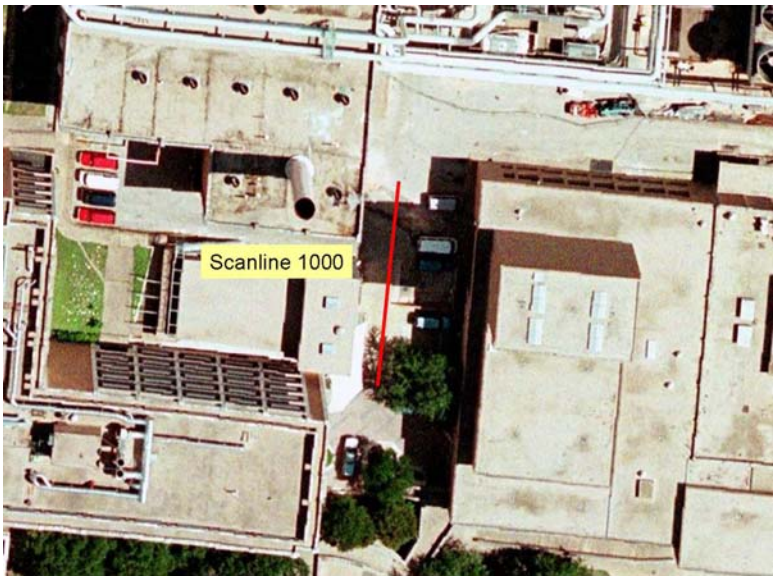

Sample	K0 (cm/s)
1001	2.8E-03
1002	0.0E+00
1003	0.0E+00
1004	1.1E-04
1005	1.3E-03
1006	1.5E-03
1007	0.0E+00
1008	3.7E-03
1009	0.0E+00
1010	1.1E-04
1011	0.0E+00
1012	5.7E-05
1013	4.5E-04
1014	1.7E-04
1015	5.7E-05
1016	5.7E-05
1017	1.7E-04
Scan Line K (cm/s)	4.9E-05

Figure 25: Site map (from Google Maps) and site photo looking south, of scanline 1000 located on a concrete and asphalt portion of the east parking lot of the geology building on the campus of The University of Texas at Austin, Texas.

Sample	K0 (cm/s)
6001	4.0E-05
6002	5.2E-04
6003	4.0E-04
6004	2.9E-03
6005	1.1E-03
6006	1.2E-04
6007	4.4E-04
6008	6.0E-04
6009	2.0E-04
6010	0.0E+00
Scan Line K (cm/s)	2.9E-05

Figure 26: Site map (from Google Maps) and site photo looking north, of scanline 6000 located on a concrete gutter section of pavement at 56th Street and Link Avenue, Austin, Texas.

Sample	K0 (cm/s)
7001	7.2E-04
7002	5.6E-04
7003	2.1E-03
7004	6.0E-04
7005	1.8E-03
7006	4.0E-04
7007	1.5E-03
7008	5.6E-04
7009	9.9E-04
7010	9.5E-04
7011	1.7E-03
7012	1.7E-03
7013	1.7E-03
7014	0.0E+00
Scan Line K (cm/s)	7.1E-05

Figure 27: Site map (from Google Maps) and site photo looking west, of scanline 7000 located on an asphalt portion of the east parking lot of The University of Texas Intramural Fields, Austin, Texas.

Sample	K0 (cm/s)
8001	6.8E-04
8002	1.7E-03
8003	1.2E-03
8004	0.0E+00
8005	1.3E-03
8006	2.8E-04
8007	8.4E-04
8008	1.2E-04
8009	0.0E+00
Scan Line K (cm/s)	2.9E-05

Figure 28: Site map (from Google Maps) and site photo looking north, of scanline 8000 located on an asphalt road at 56th Street and Link Avenue, Austin, Texas.

Sample	K0 (cm/s)
9001	0.0E+00
9002	1.2E-04
9003	2.8E-04
9004	4.0E-04
9005	2.8E-04
9006	8.0E-05
9007	0.0E+00
9008	8.0E-05
9009	0.0E+00
9010	0.0E+00
9011	1.2E-04
9012	8.0E-05
9013	4.8E-04
9014	1.2E-04
9015	8.0E-05
9016	1.6E-04
9017	8.0E-05
9018	1.2E-04
9019	3.0E-03
9020	2.4E-03
9021	1.0E-02
Scan Line K (cm/s)	8.5E-05

Figure 29: Site map (from Google Maps) and site photo looking west, of scanline 9000 located on a concrete section of the west parking lot of Hyde Park Grocery at Avenue H and 43rd Street, Austin, Texas.

Sample	K0 (cm/s)
10001	4.8E-04
10002	3.6E-04
10003	0.0E+00
10004	3.2E-04
10005	3.6E-04
10006	4.0E-05
10007	0.0E+00
10008	1.2E-04
10009	8.6E-04
10010	4.0E-05
10011	0.0E+00
10012	4.0E-05
10013	4.0E-05
10014	5.6E-04
10015	4.0E-05
Scan Line K (cm/s)	1.5E-05

Figure 30: Site map (from Google Maps) and site photo looking west, of scanline 10000 located on a concrete curb gutter at 56th Street and Duval Street, Austin, Texas.

Sample	K0 (cm/s)
11001	0.0E+00
11002	4.0E-05
11003	4.4E-04
11004	0.0E+00
11005	4.0E-05
11006	0.0E+00
11007	0.0E+00
11008	0.0E+00
11009	4.0E-05
11010	0.0E+00
11011	0.0E+00
Scan Line K (cm/s)	2.6E-06

Figure 31: Site map (from Google Maps) and site photo looking east, of scanline 11000 located on a section of concrete road at 34th Street and Tom Green Street, Austin, Texas.

Sample	K0 (cm/s)
12001	7.2E-04
12002	9.1E-04
12003	5.2E-04
12004	0.0E+00
12005	0.0E+00
12006	0.0E+00
12007	0.0E+00
12008	0.0E+00
12009	0.0E+00
12010	0.0E+00
12011	0.0E+00
12012	3.2E-04
12013	0.0E+00
Scan Line K (cm/s)	1.2E-05

Figure 32: Site map (from Google Maps) and site photo looking east, of scanline 12000 located on a section of asphalt road at 400 Swanee Drive, Austin, Texas..

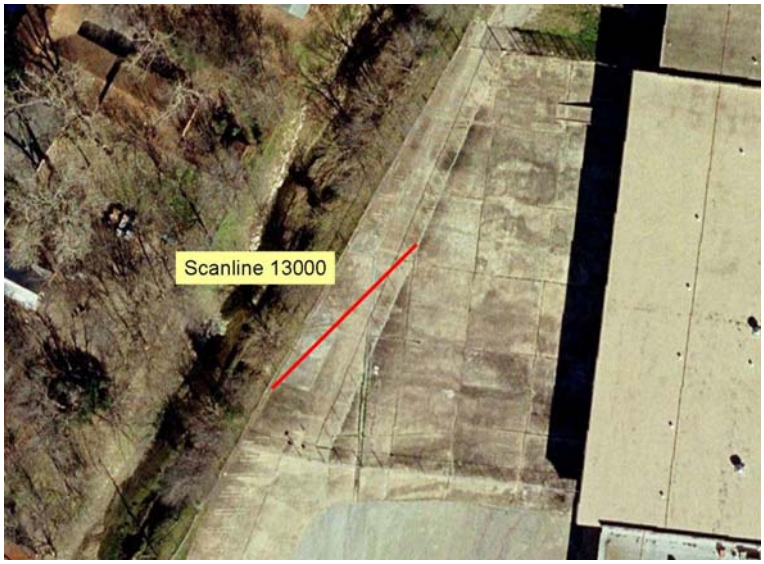

Sample	K0 (cm/s)
13001	1.0E-03
13002	1.3E-03
13003	5.6E-04
13004	6.6E-03
13005	5.2E-03
13006	0.0E+00
13007	0.0E+00
13008	2.4E-04
13009	4.8E-04
13010	2.2E-03
13011	3.4E-03
13012	2.8E-03
Scan Line K (cm/s)	1.1E-04

Figure 33: Site map (from Google Maps) and site photo looking north, of scanline 13000 located on a concrete parking lot at Denson Drive 200 feet east of Chesterfield Avenue, Austin, Texas.

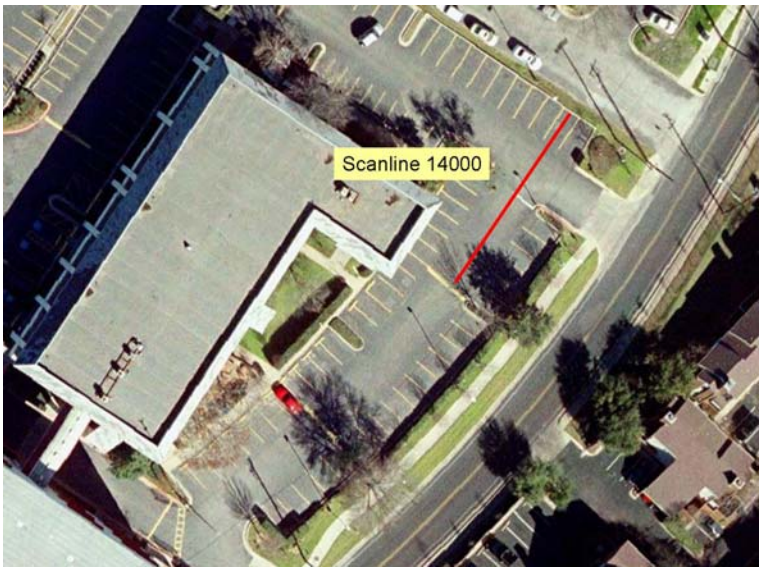

Sample	K0 (cm/s)
14001	5.6E-03
14002	2.4E-04
14003	8.0E-05
14004	7.2E-04
14005	1.2E-04
14006	4.8E-04
14007	4.0E-04
14008	3.2E-04
Scan Line K (cm/s)	3.7E-05

Figure 34: Site map (from Google Maps) and site photo north, of scanline 14000 located on an asphalt parking lot at the corner of Guadalupe Street and Northway Drive, Austin, Texas.

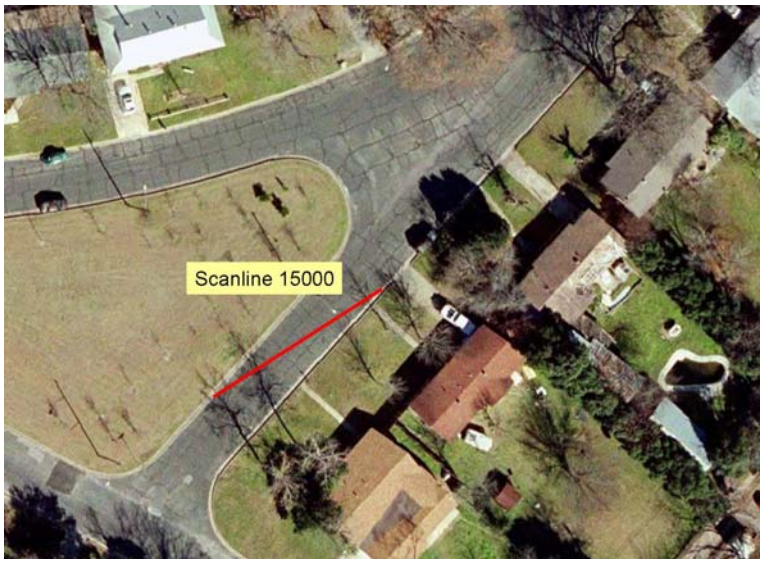

Sample	K0 (cm/s)
15001	3.0E-03
15002	0.0E+00
15003	0.0E+00
15004	8.0E-05
15005	0.0E+00
15006	0.0E+00
15007	3.2E-04
15008	0.0E+00
15009	0.0E+00
15010	8.0E-04
15011	0.0E+00
15012	6.4E-04
15013	4.4E-04
15014	0.0E+00
Scan Line K (cm/s)	2.5E-05

Figure 35: Site map (from Google Maps) and site photo looking south, of scanline 15000 located on a section of asphalt road at Meadowview Lane and Crestland Drive, Austin, Texas.

Sample	K0 (cm/s)
16001	1.4E-03
16002	4.4E-04
16003	2.0E-04
16004	1.6E-04
16005	8.0E-05
16006	0.0E+00
16007	7.2E-04
16008	4.0E-04
16009	0.0E+00
Scan Line K (cm/s)	1.6E-05

Figure 36: Site map (from Google Maps) and site photo looking south, of scanline 16000 located on a concrete curb gutter at Rowena Street and 51st Street, Austin, Texas.

Sample	K0 (cm/s)
17001	2.2E-03
17002	0.0E+00
17003	1.2E-04
17004	0.0E+00
17005	0.0E+00
17006	8.0E-05
17007	0.0E+00
17008	2.4E-04
17009	3.2E-04
17010	0.0E+00
17011	2.8E-04
17012	2.2E-03
17013	0.0E+00
17014	0.0E+00
Scan Line K (cm/s)	2.5E-05

Figure 37: Site map (from Google Maps) and site photo looking south, of scanline 17000 located on a concrete curb gutter at 40th Street and Avenue F, Austin, Texas.

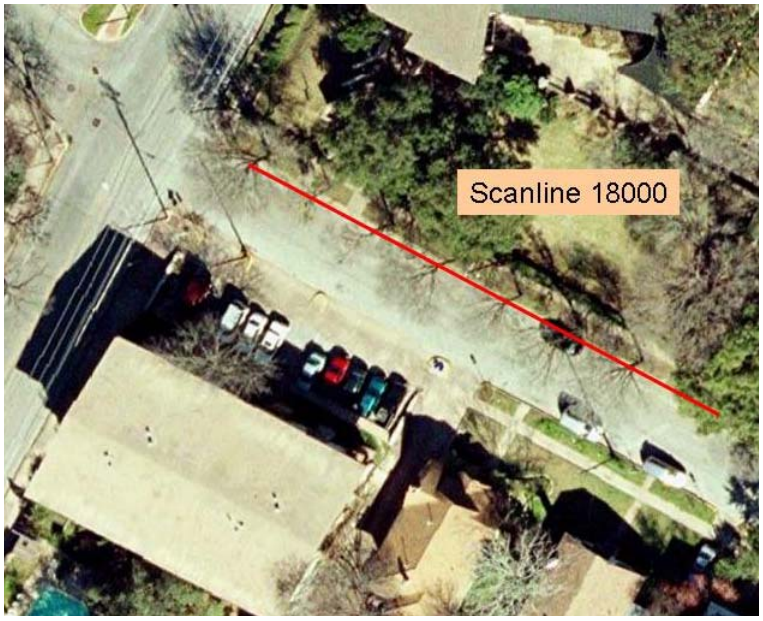

Sample	K0 (cm/s)
18001	0.0E+00
18002	0.0E+00
18003	7.2E-04
18004	0.0E+00
18005	8.0E-05
18006	0.0E+00
18007	4.0E-04
18008	2.0E-03
18009	1.6E-04
18010	0.0E+00
18011	1.5E-03
Scan Line K (cm/s)	2.2E-05

Figure 38: Site map (from Google Maps) and site photo looking west of scanline 18000 located on a concrete curb gutter at Duval Street and 31st Street, Austin, Texas.

Sample	K0 (cm/s)
19001	4.4E-03
19002	6.7E-02
19003	6.8E-03
19004	8.0E-05
19005	8.0E-04
19006	0.0E+00
19007	1.5E-03
19008	4.4E-03
19009	0.0E+00
19010	2.8E-03
Scan Line K (cm/s)	4.1E-04

Figure 39: Site map (from Google Maps) and site photo looking north, of scanline 19000 located on a concrete curb gutter at Avenue G and 40th Street, Austin, Texas.

Sample	K0 (cm/s)
20001	0.0E+00
20002	1.6E-04
20003	0.0E+00
20004	0.0E+00
20005	0.0E+00
20006	0.0E+00
20007	0.0E+00
20008	0.0E+00
20009	0.0E+00
20010	5.3E-04
Scan Line K (cm/s)	3.2E-06

Figure 40: Site map (from Google Maps) and site photo looking east, of scanline 20000 located on a concrete curb gutter at 44th Street and Avenue G, Austin, Texas.

REFERENCES

Appleby, F.V., 1937, Impervious factors: Proceedings of the Institution of Municipal and County Engineers, v. 63, p. 1077-1100.

Appleyard, S. J., Commander, D.P., and Davidson, W.A., 1999, The effects of urban development on the utilization of groundwater resources in Perth, Western Australia, *in* Chilton, J. ed., Groundwater in the urban environment – Selected City Profiles: Rotterdam, A.A. Balkema, p. 97-104.

Asquith, W.H., and Roussel, M.C., 2003, Atlas of interoccurrence intervals for selected thresholds of daily precipitation in Texas: U.S. Geological Survey Water-Resource Investigations 03-4281, 204 p.

Asquith, W.H., and Roussel, M.C., 2004, Atlas of depth-duration frequency of precipitation annual maxima for Texas: U.S. Geological Survey Scientific Investigations Report 2004-5041, 106 p.

Asquith, W.H., and Roussel, M.C., 2007, An initial-abstraction constant-loss model for unit hydrograph modeling for applicable watersheds in Texas: written communication, work in progress.

Asquith, W.H., Roussel, M.C., Thompson, D.B., Cleveland, T.G., and Fang, X., 2005, Summary of Dimensionless Texas Hyetographs and Distribution of Storm Depth Developed for Texas Department of Transportation Research Project 0-4194: U.S. Geological Survey Report 0-4194-4, 68 p.

Asquith, W.H., and Roussel, M.C., Cleveland, T.G., Fang, Xing, and Thompson, D.B., 2006, Statistical characteristics of storm inter-event time, depth, and duration for eastern New Mexico, Oklahoma, and Texas: U.S. Geological Survey Professional Paper 1725, 299 p.

Bear, J., 1972, Dynamics of Fluids in Porous Media: New York, Elsevier Publishing Company, Inc., 764 p.

Bomar, G.W., 1995, Texas weather: Austin, University of Texas Press, 275 p.

Colyer, P., 1983, Urban hydrology and catchment research in the United Kingdom – Progress since 1979, *in* Delleur, J.W. and Torno, H.C., eds., Urban hydrology: Proceedings of the International Symposium: American Society of Civil Engineers, p. 38-53.

Davies, H., and Hollis, T., 1981, Measurements of rainfall runoff volume relationships and water balance for roofs and roads, *in* Yen, B.C., ed., Urban storm water hydraulics and hydrology, Second International Conference on Urban Storm Dainage: Urbana, p. 434-443.

De Vries, J.J., and Simmers, I., 2002, Groundwater recharge: An overview of processes and challenges: Hydrogeology Journal, v. 10. p. 5-17.

Falk, J., and Niemczynowicz, K., 1978, Characteristics of the above-ground runoff in sewered catchments, *in* Helliwell, P., ed., Urban storm drainage: Pentech Press, p. 159-171.

Garcia-Fresca, B., 2004, Urban effects on groundwater recharge in Austin, Texas [MS thesis]: Austin, The University of Texas, 173 p.

Garcia-Fresca, B., and Sharp, J.M. Jr., 2005, Hydrogeologic considerations of urban development: Urban induced recharge, *in* Ehlen, J., et al., eds., Humans as Geologic Agents: Boulder, Geological Society of America Reviews in Engineering Geology, v. XVI, p. 123-136.

Gee, G.W., Wierenga, P.J., Andraski, B.J., Young, M.H., Fayer, M.J., and Rockhold, M.L., 1994, Variations in water balance and recharge potential at three western desert sites: Soil Science Society of America Journal, v. 58, p. 82-96.

Halihan, T., Sharp, J.M. Jr., and Mace, R.E., 1999, Interpreting flow using permeability at multiple scales, in Palmer, A.R., et al., eds., Karst modeling. Karst waters insititute special publication no. 5: Charlottesville, p. 82-96.

Hollis, G.E., and Ovenden, J.C., 1988a, The quantity of runoff from ten stretches of road, a car park and eight roofs in Herfordshire, England during 1983: Hydrological Processes, v. 2, p. 227-243.

Hollis, G.E., and Ovenden, J.C., 1988b, One year irrigation experiment to assess losses and runoff volume relationships for a residential road in Herfordshire, England during 1983: Hydrological Processes, v. 2, p. 61-74.

Hooke, R.L., 1994, On the effect of humans as geomorphic agents: GSA Today, v. 4, no. 9, p. 217-225.

Hooke, R.L., 2000, On the history of humans as geomorphic agents: Geology, v. 28, no. 9, p. 843-846.

Hooker, P.J., McBridge, D., Brown, M.J., Lawrence, A.R., and Gooddy, D.C., 1999, An integrated hydrogeological case study of a post-industrial city in the west Midlands of England, *in* Chilton, J. ed., Groundwater in the urban environment – Selected City Profiles: Rotterdam, A.A. Balkema, p. 145-150.

Kidd, C.H.R., 1978, Rainfall-runoff processes over urban surfaces: Institute of hydrology report no. 53, 84 p.

Kiraly, L., 1975, Rapport sur l'etat actuel des connaissances dans le domaine des caracteres physiques des roches karstiques, *in* Burger, A. and Dubertret, L., eds., Hyddrogeology of karstic terrains: Paris, International Association of Hydrogeologists, series B, no. 3, p. 53-67.

Krothe, J.M., 2002, Effects of urbanization on hydrogeological systems: The physical effects of utility trenches [MS thesis]: Austin, The University of Texas at Austin, 190 p.

Kuichling, E., 1909, Report on the adequacy of the existing sewerage systems of the Black Bay district of Boston: USA, *in* Watkins, 1962.

Lee, J.G., and Heaney, J.P., 2003, Estimation of urban imperviousness and its impacts on storm water systems: Journal of Water Resource Planning and Management, v. 129, issue 5, p. 419-426.

Lerner, D.N., 1990, Groundwater recharge in urban areas, in Massing, H., et al., eds., Hydrological processes and water management *in* Urban areas: Wallingford, International Association of Hydrological Sciences, Publication no. 198, p. 59-65.

Lerner, D.N., 1997a, Groundwater recharge, in Saether, O.M., and de Caritat, P., eds., Geochemical processes, weathering and groundwater recharge in catchments: Rotterdam, A.A. Balkema, p. 109-150.

Lerner, D.N., 1997b, Too much or too little: recharge in urban areas, in Chilton, J., et al., eds., Proceedings of the twenty-seventh congress of the International Association of Hydrogeologists: Rotterdam, A.A. Balkema, p. 41-47.

Lerner, D.N., 2002, Identifyling and quantifying urban recharge: a review: Hydrogeology Journal, v. 10, p. 143-152.

Lloyd-Davies, D.E., 1906, The elimination of storm water from sewage systems, Proc., Inst. Civ. Eng., London, 164, p. 44-67.

Marrett, R., 1996, Aggregate properties of fracture populations: Journal of Structural Geology, v. 18, no. 213, p. 169-178.

Pratt, C.J., and Henderson, R.J., 1981, Overland flow and catchment characteristics, *in* Urban storm drainage: Hydraulics and hydrology: Proceedings of the second international conference, Urbana, University of Illinois, p. 83-92.

Ragab, R., Rosier, P, Dixon, A., Bromley, J., and Coop, J.P., 2003, Expeirmental study of water fluxes in a residential aea: 2. road infiltration, runoff and evaportation: Hydrological Processes, vo. 17, no. 12, p. 2423-2437.

Scanlon, B.R., Healy, R.W., and Cook, P.G., 2002, Choosing appropriate techniques for quantifying groundwater recharge: Hydrogeology Journal, v. 10, p. 18-39.

Schueler, T.J., 1994, Importance of imperviousness: Watershed protection techniques, v. 1, p. 100-111.

Sherlock, R.L., 1922, Man as a geological agent: an account of his action on inanimate nature: London, H.F.&G. Witherby, 372 p.

Sharp, J.M. Jr., 1993, Fractured aquifers/reservoirs: approaches, problems, and opportunities, in Banks, D., and Banks, S., eds., Hydrogeology of hard rocks. Memoire of the XXIV Congress: Oslo, International Association of Hydrogeologists, v. 24, no. 1, p. 23-38.

Sharp, J.M. Jr., 1997, Ground-water supply issues in urban and urbanizing areas, *in* Chilton, J., et al., eds., Groundwater in the urban environment: Problems, processes and management: Rotterdam, A.A. Balkema, p. 67-74.

Sharp, J.M. Jr., Hansen, J.M., and Krothe, J.N., 2001, Effects of urbanization on hydrogeological systems: The physical effects of utility trenches, in Seiler, K.P., and Wohnlich, S., eds., New approaches characterizing groundwater flow: Proceedings of the International Association of Hydrogeologists XXXI Congress, Munich, supplement volume, 4 p.

Sharp, J.M. Jr., Krothe, J., Mather, J.D., Garcia-Fresca, B., and Stewart, C.A., 2003, Effects of urbanization on groundwater systems, *in* Heiken, G., et al., eds., Earth sciences in the city: a reader: Washington D.C., American Geophysical Union, p. 257-278.

Simmers, I., 1998, Groundwater recharge: an overview of estimation ‘problems’ and recent developments, in Robins, N.S., ed., Groundwater pollution, aquifer recharge and vulnerability: London, Geological Society Special Publication no. 130. p. 107-115.

Soil Conservation Service, 1973, A method for estimating volume and rate of runoff in small watersheds: SCS-TP-149, U.S. Department of Agriculture, Soil Conservation Service, 19 p.

Stephens, D.B., 1994, A perspective on diffuse natural recharge mechanisms in areas of low precipitation: Soil Science Society of America Journal, v. 58, p. 40-48.

Stephenson, D., 1994, Comparison of the water balance for an undeveloped and suburban catchment: Hydrological Sciences, v. 39, p. 295-307.

van Dam, C.H., and van de Ven, F.H.M., 1984, Infiltration in the pavement, in Balmer, P., et al., eds., Proceedings of the Third International Conference on Urban Storm Drainage: Gothenberg, p.1019-1028.

van de Ven, F.H.M., 1990, Water balances in urban areas, *in* Massing, H., et al., eds., Hydrological processes and water management in urban areas: Wallingford, International Association of Hydrological Sciences Publication no. 198, p. 21-32.

Watkins, L.H., 1962, The design of urban sewer systems: research into the relation between the rate of rainfall and the rate of flow in sewers: Road Research Technical Paper No. 55, HMSO London, 96 p.

Zondervan, J.G., 1978, Modeling urban runoff: a quasilinear approach: Wageningen Agricultural Research Report 874, 68 p.

This document does not include the vita page from the original.